Research Article | Vol. 29, No. 14 / 5 July 2021 / Optics Express 21084
Optics EXPRESS

High latitude Southern Ocean phytoplankton have distinctive bio-optical properties

CHARLOTTE M. ROBINSON,[1,*] YANNICK HUOT,[2] NINA SCHUBACK,[1,3,4] THOMAS J. RYAN-KEOGH,[5] SANDY J. THOMALLA,[5,6] AND DAVID ANTOINE[1,7]

[1]*Remote Sensing and Satellite Research Group, School of Earth and Planetary Sciences, Curtin University, Kent Street, Bentley, WA 6102, Australia*
[2]*Centre d'Applications et de Recherches en Télédétection, Département de géomatique appliquée, Université de Sherbrooke, Sherbrooke, Québec J1K 2R1, Canada*
[3]*Swiss Polar Institute, École Polytechnique Fédérale de Lausanne, Lausanne, Switzerland*
[4]*Institude of Geological Sciences and Oeschger Center for Climate Change Research, University of Bern, Bern, Switzerland*
[5]*Southern Ocean Carbon and Climate Observatory (SOCCO), Smart Places, CSIR, Rosebank, Cape Town 7700, South Africa*
[6]*Marine Research Institute (MaRe), University of Cape Town, Rondebosch, Cape Town 7701, South Africa*
[7]*Sorbonne Université, CNRS, Laboratoire d'Océanographie de Villefranche, Villefranche sur mer 06230, France*
[*]*charlotte.mary.robinson@gmail.com*

Abstract: Studying the biogeochemistry of the Southern Ocean using remote sensing relies on accurate interpretation of ocean colour through bio-optical and biogeochemical relationships between quantities and properties of interest. During the Antarctic Circumnavigation Expedition of the 2016/2017 Austral Summer, we collected a spatially comprehensive dataset of phytoplankton pigment concentrations, particulate absorption and particle size distribution and compared simple bio-optical and particle property relationships as a function of chlorophyll *a*. Similar to previous studies we find that the chlorophyll-specific phytoplankton absorption coefficient is significantly lower than in other oceans at comparable chlorophyll concentrations. This appears to be driven in part by lower concentrations of accessory pigments per unit chlorophyll *a* as well as increased pigment packaging due to relatively larger sized phytoplankton at low chlorophyll *a* than is typically observed in other oceans. We find that the contribution of microphytoplankton (>20 μm size) to chlorophyll *a* estimates of phytoplankton biomass is significantly higher than expected for the given chlorophyll *a* concentration, especially in higher latitudes south of the Southern Antarctic Circumpolar Current Front. Phytoplankton pigments are more packaged in larger cells, which resulted in a flattening of phytoplankton spectra as measured in these samples when compared to other ocean regions with similar chlorophyll *a* concentration. Additionally, we find that at high latitude locations in the Southern Ocean, pheopigment concentrations can exceed mono-vinyl chlorophyll *a* concentrations. Finally, we observed very different relationships between particle volume and chlorophyll *a* concentrations in high and low latitude Southern Ocean waters, driven by differences in phytoplankton community composition and acclimation to environmental conditions and varying contribution of non-algal particles to the particulate matter. Our data confirm that, as previously suggested, the relationships between bio-optical properties and chlorophyll *a* in the Southern Ocean are different to other oceans. In addition, distinct bio-optical properties were evident between high and low latitude regions of the Southern Ocean basin. Here we provide a region-specific set of power law functions describing the phytoplankton absorption spectrum as a function of chlorophyll *a*.

#426737 https://doi.org/10.1364/OE.426737
Journal © 2021 Received 7 Apr 2021; revised 28 May 2021; accepted 28 May 2021; published 21 Jun 2021

Optics EXPRESS

1. Introduction

The Southern Ocean (SO), defined here as the waters south of the Subtropical Front, is a significant CO_2 sink [1,2] which is undergoing physical and chemical changes from ocean warming, acidification, and freshening from increased sea-ice melt [3,4]. These environmental pressures will in turn alter the present and future physiology, abundance and community structure of phytoplankton [3,5], the photosynthetic microbes underpinning the biological carbon pump (BCP). Given the vastness and remoteness of the SO, ocean colour remote sensing is an important tool for observing changes in SO phytoplankton [6–9]. However, interpreting ocean colour data relies on robust relationships between the remotely measured signal, the *in situ* optical properties and the biogeochemical properties of interest. Consequently, substantial field sampling and the collection of both *in situ* biological and bio-optical datasets are essential to the application of ocean color remote sensing approaches. An additional benefit of establishing robust relationships is that by measuring one observable variable–for example the chlorophyll *a* concentration at the surface which can be achieved with ocean color remote sensing–further information can be inferred about correlated parameters like phytoplankton community composition, average size, or vertical distribution [10,11], all of which have implications for ecosystem function and the efficiency of the BCP.

When sunlight enters the surface ocean, it is absorbed and scattered by particles (phytoplankton and other non-algal particles), coloured dissolved organic matter (CDOM) and water, and partially scattered back out of the surface ocean with a spectrum that is different to that of the incoming sunlight [12]. The spectra of light exiting the surface ocean and its overall intensity, commonly referred to as *ocean colour*, is therefore dependent on the relative composition, abundance, and size (for particles) of the dissolved or particulate material in the surface ocean [13]. Empirical relationships between the ocean colour spectrum and bio-optical properties of optically active constituents (phytoplankton, CDOM, non-algal particles), or biogeochemical properties, enable us to deconvolve the ocean colour spectrum into useful quantities such as chlorophyll *a* concentration. Relationships between bio-optical properties (e.g., absorption), biogeochemical quantities (e.g., chlorophyll *a* concentration), and community characteristics (e.g., phytoplankton species or size), are however not uniform throughout the World Ocean [14]. Variability in these relationships can be expected on both regional and temporal scales driven by differences in phytoplankton species composition and changes in the availability of essential resources for phytoplankton growth such as light and nutrients [15,16].

Generally there is a paucity of *in situ* bio-optical and matched biogeochemical data in the SO, as compared to other ocean basins. Measurements are temporally constrained to the summer season and spatially constrained to a few areas of interest. Areas such as the Antarctic Peninsula, Kerguelen Plateau, Sub-Antarctic and Polar Frontal Zones of the Indian Ocean, Ross Sea and Scotia Seas are comparatively well sampled for properties such as pigment concentration and particulate absorption compared to other areas of the Southern Ocean [17–21]. However these areas represent only a fraction of the spatial extent of the SO and a mere glimpse into the optical properties of the many different biomes within the SO [6]. Areas such as open ocean waters of the high latitudes (South of 60°S) have been particularly undersampled, specifically the Bellinghausen and Amundsen Seas [22], and also the low latitudes of the Atlantic Ocean sector.

Past studies have shown that the bio-optical properties of phytoplankton within the SO are different to other oceans [18,23,24]. For example the chlorophyll-specific absorption coefficient (a^*) has been reported to be considerably lower than values in low- and mid-latitude oceans at comparable chlorophyll *a* concentrations [18]. The lower a^* was typically due to increased pigment packaging, resulting from acclimation to low *in situ* light intensities and/or larger cell size [18,25]. However, large variations in both the absolute values and range of values of a^* has been observed in the Southern Ocean [26], sometimes within the same region [20,25]. Some of this disparity is explained by methodological differences such as the choice of pathlength

Optics EXPRESS

amplification factors for the particulate absorption measurements [18,20]. Other factors, such as spatial and seasonal availability of light and nutrients [27], and phytoplankton species composition [26,28–30], leading to variations in cell sizes and pigment composition [31,32], have been identified as being important determinants. Overall, there are still fundamental gaps in our understanding of if, how and why Southern Ocean bio-optical and biogeochemical relationships differ from other oceans.

The SO is a unique environment for phytoplankton due to its strong circumpolar ocean currents and seasonal or permanent ice zones which create hydrographic boundaries that divide the surface ocean [33], where phytoplankton reside, into oceanic zones of distinct physical and chemical properties [34]. Environmental factors which influence phytoplankton growth and species selection such as temperature, light availability and dissolved nutrient composition and concentrations differ [35], both within and between regions. For example in the Subantarctic Zone, low silicic acid favours a more diverse community of typically nano- (2-20 μm) and pico- (<2 μm) sized phytoplankton [36,37], while further south, below the Polar Front, increased nitrate, phosphate and silicic acid encourage the growth of microphytoplankton (>20 μm), specifically diatoms, which tend to dominate the phytoplankton community [28,36,38,39]. Across the entire SO, phytoplankton are typically co-limited by light, dissolved iron and silicic acid [40]. The dominant species of a bloom in response to increases in light, iron or silicic acid, can vary with location and change over time [41].

The Antarctic Circumnavigation Expedition (ACE) presented an opportunity to collect the most spatially extensive SO dataset for investigating the relationship between phytoplankton particulate absorption, pigments and particle size. Specifically, we investigated the variations in phytoplankton pigments and community composition with chlorophyll *a* and pheopigment concentration and the impact on the phytoplankton absorption coefficients. We also looked into the changes in particle volume as a function of chlorophyll *a*. The results from this study provide a set of chlorophyll-specific particulate absorption coefficients for modelling phytoplankton abundance and particulate absorption in this region.

2. Methods

2.1. Study area and sampling

Samples were collected during legs 1-3 of the ACE expedition (see Walton and Thomas [42]) aboard the *RV* Akademik Tryoshnikov during the Austral Summer from 20 December 2016-19 March 2017. Legs 1-3 of the expedition travelled east around the Southern Ocean from Cape Town, South Africa, through the Indian Ocean to Hobart, Australia (leg 1), via the Pacific Ocean to Punta Arenas, Chile (leg 2), and through the Atlantic Ocean back to Cape Town (leg 3). During legs 1 and 3, the ship's meridional position remained within approximately 40 to 60° S, venturing further south to almost 80° S during leg 2 (Fig. 1). In addition, a number of subantarctic islands and the Antarctic continent were visited. Most locations are highlighted in Fig. 1. The voyage GPS track and other datasets cited here are available at https://zenodo.org/communities/spi-ace. Samples for particulate absorption, pigment analysis and particle size distribution were collected from the underwater seawater supply (Grundfos Lenntech centrifugal pump) fixed at 4.5 m every 3-6 hours.

2.2. Physical oceanography

A thermosalinograph (Chelsea Technologies AquaLine Ferrybox system) connected to the underway seawater supply collected a semi-continuous record of sea surface temperature (SST; °C) and salinity of the surface ocean (data available at [43]).

The mixed layer depth (MLD; m) at each sampling point was retrieved by linearly interpolating the climatological monthly MLD means from de Boyer Montégut et al. [44] to the sampling dates.

Optics EXPRESS

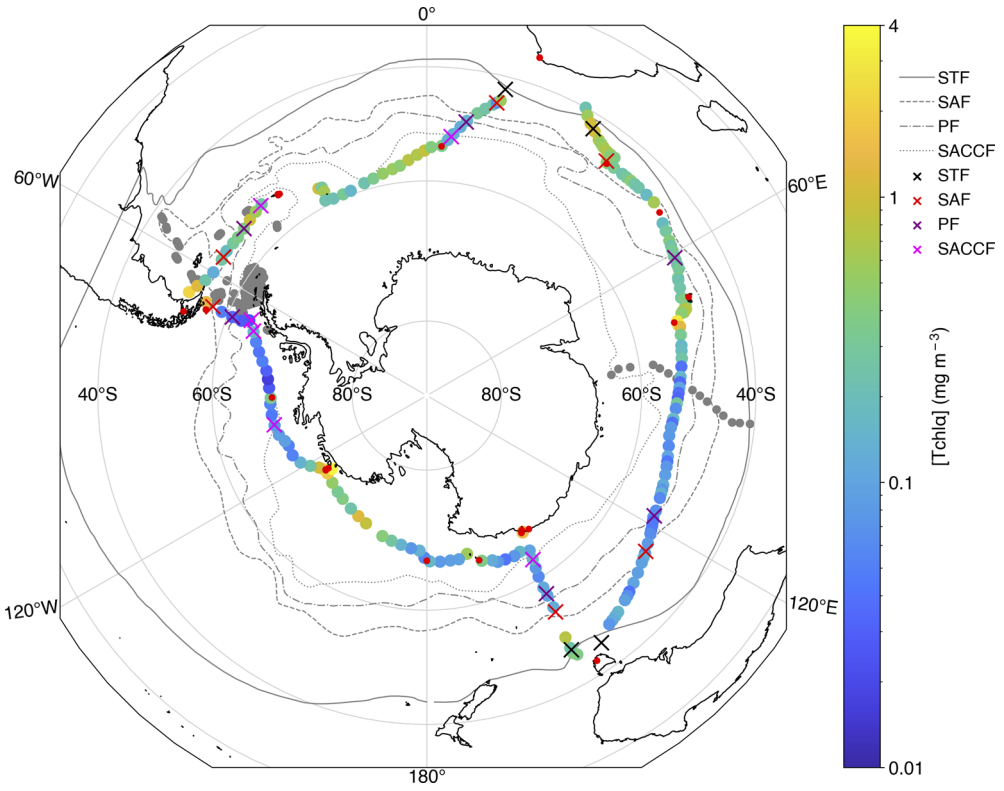

Fig. 1. Map of underway sampling points during ACE legs 1-3, colourmapped with [Tchl*a*] (sum of monovinyl-chlorophyll *a*, divinyl-chlorophyll *a*, chlorophyll *a* epimers, chlorophyll *a* isomers and chlorophyllide *a* concentrations). Grey points indicate location of samples extracted from the NOMAD dataset. Red points indicate island locations. Locations of the major fronts along the track identified *in situ* data [43] are marked with 'X' markers. Dashed lines in background are the climatological positions of the major Southern Ocean fronts from Orsi et al. [33]. STF = Subtropical Front, SAF = Subantarctic Front, PF = Polar Front, SACCF = Southern Antarctic Circumpolar Current Front.

The MLDs were derived using the density threshold method (depth where σ_θ=$\sigma_{\theta_{10m}}$+/-0.03 kg m^{-3}; [44]; Fig. 2). The MLD was additionally calculated using density profiles derived from conductivity-temperature-depth (CTD; [45]) casts. However those measurements were sporadic and cannot be interpolated meaningfully along the complete ship transit. A comparison of the CTD derived estimates and climatology estimates show a very similar pattern across the timeseries (CTD=1.1x - 12, R^2 = 0.6, p<0.05).

The depth of the euphotic zone (Z_{eu}; m) was derived as a polynomial expression of [Tchl*a*] (sum of monovinyl-chlorophyll *a*, divinyl-chlorophyll *a*, chlorophyll *a* epimers, chlorophyll *a* isomers and chlorophyllide *a* concentrations) at the surface [Tchla_{surf}] (mg m^{-3}; equation from Fig. 9 in Morel et al. [46]):

$$\log_{10}Z_{eu} = 1.524 - 0.0460[\text{Tchl}a_{surf}] - 0.00051[\text{Tchl}a_{surf}]^2 + 0.0282[\text{Tchl}a_{surf}]^3. \quad (1)$$

The ratio between the depth of Z_{eu} and MLD provides a crude indication of the water column mixing regime experienced by phytoplankton where Z_{eu}/MLD < 1 means that the mixing layer depth is deeper than the whole euphotic zone indicating well-mixed waters, while Z_{eu}/MLD > 1 suggests a stratified water column where the euphotic zone extends below the mixed layer [10].

Optics EXPRESS

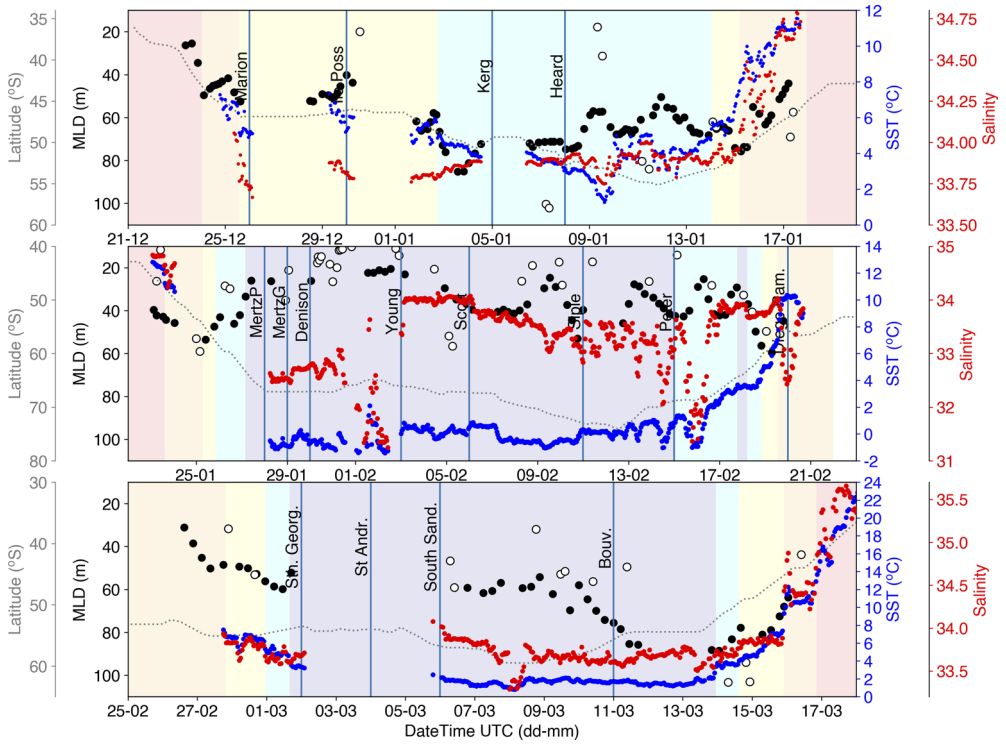

Fig. 2. Timeseries of leg 1 (top), leg 2 (middle) and leg 3 (bottom) showing latitude (°S; dotted grey line), mixed layer depth (MLD (m) from the de Boyer Montégut et al. [44] density threshold climatology; black circles), MLD from *in situ* CTD casts; open black circles, sea surface temperature (°C; blue circles) and salinity (red circles) from the underway Ferrybox. Some island visits are indicated by labelled blue lines. Background colours of indicate the ocean zones between major ocean fronts from [43] where red = STZ, orange=SAZ, yellow=PFZ, cyan=AZ, purple=MIZ. See text in *Physical Oceanography* section for definitions.

Frontal positions from *in situ* data [43] and the climatological means of Orsi et al. [33] are plotted to aid interpretation of the results (Figs. 1 and 2). The positions of the Subtropical Front (STF), Subantarctic Front (SAF), Polar Front (PF) and the Southern Antarctic Circumpolar Current Front (SACCF) were derived *in situ* by identifying strong lateral gradients in temperature, salinity or sea surface height and were in close proximity to their climatological mean positions [33]. Oceanic zones are defined as the Subtropical Zone, north of the STF, the Subantarctic Zone (SAZ) between the the STF and SAF, the Polar Frontal Zone (PFZ) between the SAF and PF, the Antarctic Zone (AZ) between the PF and SACCF, and the Marginal Ice Zone (MIZ), south of the SACCF.

The median light intensity within the mixed layer, I_g (μmol photons m^2 s^{-1}) was estimated for each sample. First the light attenuation coefficient K_dPAR (m^{-1}) was calculated as per Morel [47]. For each sample, the average instantaneous PAR over the previous 72 hours (avPAR(0)) in μmol photons m^2 s^{-1} was calculated from 1 min resolution above-water PAR measurements [48]. At each sample point, the average PAR at 1 metre (z) intervals between the surface and mixed layer depth was calculated as per [49]

$$avPAR(z) = avPAR(0)e^{K_dPAR \times z} \tag{2}$$

Finally I_g was calculated as the median avPAR(z) within the mixed later.

Optics EXPRESS

2.3. Phytoplankton pigments

Particles from up to 2 L of seawater were collected on 0.7 μm pore size 25 mm diameter glass fibre filters (GF/F; Whatman) under low vacuum pressure, immediately frozen in liquid nitrogen and stored at -80 °C for post-voyage analysis. Phytoplankton pigment concentrations were determined using high performance liquid chromatography (HPLC) following Ras et al. [50]. A full description of the pigment analysis and the data are available from Antoine et al. [51].

Following Ras et al. [50], total chlorophyll *a* [Tchl*a*] is the sum of monovinyl-chlorophyll *a*, divinyl-chlorophyll *a*, chlorophyll *a* epimers, chlorophyll *a* isomers and chlorophyllide *a* concentrations. [Pheo*a*] is the sum of the pheopigments pheophorbide *a* and pheophytin *a*, and [Tchl*a* + Pheo*a*] is the sum of [Tchl*a*] and [Pheo*a*]. [Tchl*b*] is the concentration of chlorophyll *b* only. [Tchl*c*] is the sum of chlorophyll *c*3 and chlorophyll *c*1*c*2. Concentrations of total photosynthetic [PSC] and photoprotective [PPC] pigments were also calculated where [PSC] is the sum of fucoxanthin, peridinin, 19'hexanoloxyfucoxanthin and 19'butanoloxyfucoxanthin, and [PPC] is the sum of diadinoxanthin, alloxanthin, zeaxanthin, lutein, α-carotene and β-carotene.

2.4. Filter-pad absorption measurements

Particulate absorption measurements were made (first) on the same filters analysed for pigments. A full description of the measurement protocols and the data are available at [52]. Briefly, measurements of optical density from 350-750 nm (1 nm interval) were blank corrected and converted into particulate absorption ($a_p(\lambda)$; m^{-1}). Unless specified, all chlorophyll-specific coefficients presented in this paper have been derived by dividing by [Tchl*a* + Pheo*a*].

2.4.1. Decomposition of phytoplankton and non-algal particle absorption

The phytoplankton ($a_\phi(\lambda)$; m^{-1}) and non-algal particle ($a_{nap}(\lambda)$; m^{-1}) absorption spectra were numerically decomposed using a semi-analytical inversion of the particulate absorption spectra using Bricaud et al. [53] and Bricaud et al. [54] phytoplankton chlorophyll-specific spectral shapes as the eigenvectors. Equation (3) was fitted to the particulate absorption spectra with a least squares fit with trust-reflective algorithm [55,56] in Matlab 2019b.

$$a_p(\lambda) = C_1 A_\phi(\lambda) \langle \mathrm{Chl}_{\mathrm{Bricaud}} \rangle^{E_\phi(\lambda)-1} + a_{nap}(\lambda_{ref}) e^{-S(\lambda-\lambda_{ref})} + Residual(\lambda) \quad (3)$$

where the $A_\phi(\lambda)$ and $E_\phi(\lambda)$ are the input coefficient and exponent for the power law describing phytoplankton absorption as a function of [Tchl*a* + Pheo*a*] from Bricaud et al. [53] and Bricaud et al. [54]. The remaining parameters (C_1, $\langle \mathrm{Chl}_{\mathrm{Bricaud}} \rangle$, $a_{nap}(\lambda)$, and S) are estimated by the least squares fitting process. The parameters C_1 and $\langle \mathrm{Chl}_{\mathrm{Bricaud}} \rangle$ both represent estimated values of [Tchl*a* + Pheo*a*]. However, the $\langle \mathrm{Chl}_{\mathrm{Bricaud}} \rangle$ is mostly influenced by the shape of the absorption spectrum as such, it will reflect the [Tchl*a* + Pheo*a*] at which this spectrum would be found in the Bricaud statistics in terms of shape. For example, a highly packaged spectrum at low *in situ* [Tchl*a* + Pheo*a*] will return a $\langle \mathrm{Chl}_{\mathrm{Bricaud}} \rangle$ that is higher than measured *in situ* because highly packaged spectra are found at high [Tchl*a* + Pheo*a*] in the Bricaud statistics. The parameter C_1 is the concentration of [Tchl*a* + Pheo*a*] that multiplies chlorophyll-specific phytoplankton absorption coefficient and therefore reflects the in situ [Tchl*a* + Pheo*a*] more closely. The parameter $a_{nap}(\lambda)$ is the estimated non-algal absorption at the reference wavelength (λ_{ref}) and S is the estimated spectral slope of non-algal absorption. Residuals (observations-model) from the least squares fitting process are reassigned to the phytoplankton absorption spectrum where ($a_\phi(\lambda)$; m^{-1}) is determined as Eq. (3):

$$a_\phi(\lambda) = C_1 A_\phi(\lambda) \langle \mathrm{Chl}_{\mathrm{Bricaud}} \rangle^{E_\phi(\lambda)-1} + Residual(\lambda) \quad (4)$$

Optics EXPRESS

2.5. Particle size distribution

Measurements of the particle size distribution were made on a Beckmann Multisizer 3 Coulter counter with a 100 μm aperture tube detecting particles in the range of 2-60 μm across 400 bins. Each sample constituted a cumulative analyses of 20 runs of 2000 μL each. Blank samples of 0.2 μm filtered seawater were also measured and the median blank subtracted from all whole samples (mean of 20 subsample measurements). Counts were converted to particles per m^3 and (equivalent spherical) particle volume (μm^3 m^{-3}). The diameter bins were restricted to 2-30 μm as no particles were observed in larger bins. Plots of particle concentration vs bin diameter were visually inspected and samples with high noise or particle concentrations constrained to just a few bins were flagged as poor quality and removed. The total particle volume in each sample (μm^3 m^{-3}) was derived by integrating the particle volume distribution for each sample. The mean (equivalent spherical) particle volume of each sample (μm^3) was calculated by first dividing the particle volume distribution (μm^3 m^{-3}) by the bin width (in m), before integrating to total particle volume and dividing by the particle concentration (also corrected for bin width).

2.6. Data analysis

2.6.1. Pigment and packaging indices

The contribution of three pigment-based sized classes [57,58], microphytoplankton (f_{micro}; > 20 μm, unitless), nanophytoplankton (f_{nano}; 2-20 μm, unitless), and picophytoplankton (f_{pico}; < 2 μm, unitless) to the pigment biomass were calculated according to [10].

Pigment packaging was quantified following the pigment reconstruction technique [53] to derive $a_{sol}(\lambda)$, the absorption coefficient of the same material dispersed into solution. The $a_{sol}(\lambda)$ is calculated as

$$a_{sol}(\lambda) = \Sigma C_i a^*_{sol,i}(\lambda) \tag{5}$$

where $a^*_{sol,i}$ coefficients are the weight-specific absorption spectra of individual pigments (m^2 mg^{-1}) (from Clementson and Wojtasiewicz [59]), and C_i are their concentrations in the medium (mg m^{-3}). The Clementson and Wojtasiewicz [59] dataset was selected as it includes a wide variety of accessory carotenoid pigments, as well as chlorophyll *a* degradation pigments, chlorophyllide *a*, pheophorbide *a*, and pheophytin *a*. The spectra from [59] were wavelength shifted by first correcting for the differences in refractive index between the solvent and water (i.e. multiply the wavelength by the ratio of the solvent refractive index and water refractive index) as in [60,61]. The spectra of all pigments were then shifted to *in vivo* positions to match the positions in Bricaud et al. [53] and Bidigare et al. [62]. See Supplement 1 for the wavelength corrected spectra, refractive index multipliers, and wavelength shifting information for each pigment. The pigment packaging index ($Q^*_a(\lambda)$) is calculated as

$$Q^*_a(\lambda) = a_\phi(\lambda)/a_{sol}(\lambda) \tag{6}$$

The $a_{miss}(440)$ term from Bricaud et al. [53] was not included in the $Q^*_a(440)$ calculation here as the relationship from Bricaud et al. [53] did not appear to be correct for this ACE dataset, and when applied, reduced the $Q^*_a(440)$ by 50 %.

2.6.2. Comparison data

For comparison, data from the Southern Ocean (south of 40°S) within the NASA bio-Optical Marine Algorithm Dataset v2.a (NOMAD) [63] are presented as grey symbols in some figures. The locations of these samples are constrained primarily to Drake's Passage, Scotia Sea and Antarctic Peninsula waters and along parallels between 80-90 °E in the Indian Ocean sector (Fig. 1).

The Bricaud et al. [53,54,64] datasets are used herein as comparison with our dataset. They include data from the Mediterranean Sea, North Atlantic Ocean, Benguela Upwelling and Pacific

Optics EXPRESS

Ocean. A significant fraction of the 1998 dataset, especially at high chlorophyll concentration are from the Gulf of St-Lawrence. The pigment and particulate absorption data from [53] are also included as mauve symbols in some figures for comparison. For ease of interpretation, the following acronyms have been assigned to these datasets: B98 for Bricaud et al. [64], B04 for Bricaud et al. [53] and B10 for Bricaud et al. [54].

It is noted that many bio-optical papers presenting chlorophyll-specific parameterisations and statistics vary in their definition of total chlorophyll *a* and the abbreviations or symbols used to represent the inclusion of chlorophyll *a* derivatives and pheopigments. For example the chlorophyll-specific parameters and functions of B98, B04 and B10 include pheopigments in the calculations or normalisations, whereas Uitz et al. [10] does not. As we show below, the concentration of pheopigments, pheophorbide *a* and pheophytin *a* ([Pheo*a*]) in our ACE dataset vary from 5 % to > 100 % of the [Tchl*a*]. In contrast pheopigments contributed < 5 % in the B04 dataset. Additionally, when describing the "trophic status" of a water body using the chlorophyll *a* concentration, typically this constitutes monovinyl-chlorophyll *a* and divinyl-chlorophyll *a* [57]. For these reasons, we present most bio-optical, pigment, and particle relationships as a function of, or normalised to, [Tchl*a*] only ([Tchl*a*] = monovinyl-chlorophyll *a*, divinyl-chlorophyll *a*, chlorophyll *a* epimers, chlorophyll *a* isomers and chlorophyllide *a*). However, for comparison, we do present some relationships as a function of, or normalised to, [Tchl*a* + Pheo*a*], and explicitly specify this in the results and figures.

3. Results and discussion

3.1. Physical and biological oceanography during sampling

Sea surface temperature (SST) decreased with increasing latitude (Fig. 2) as expected [34], transitioning from warmer subtropical waters with a maximum of 22°C north of the STF in the Atlantic Ocean sector, to -2°C in Antarctic waters south of the SACCF. SST ranged from 5-16°C in the SAZ, 4-10°C in the PFZ, 2-4°C in the AZ and subzero south of the SACCF (Fig. 2), typical of Austral summer conditions [65].

The MLDs from *in situ* CTD casts and from climatological monthly means of de Boyer Montégut et al. [44] are presented in Fig. 2. Overall the trends in the *in situ* and climatology datasets agree well (See section Physical Oceanography). Surface mixed layers ranged from 15 to 100 m *in situ* and 20 to 80 m in the climatology. The MLDs are noticeably shallower in the Pacific sector of the Southern Ocean, typically < 40 m, where the ship predominately surveyed waters in the MIZ south of the SACCF. Increasing sea-ice meltwater in December is known to form shallow surface mixed layers of around 20 m in the Ross and Amundsen Seas [66], which can however deepen with changes in cross-shelf advection. The deepest MLDs were observed during the time the ship was near Kerguelen and Bouvetoya Islands (Fig. 2). At both islands, a combination of changes to the bathymetry and surface advection, which can also be influenced by nearby frontal boundaries, typically results in a deepening of the MLD relative to surrounding open waters [67–69]. A deepening of the MLD at Siple Island in the climatological database were not observed in the CTD temperature profiles, which remained shallow before and after Siple Island.

The [Tchl*a*] concentrations along the ACE transit were generally low (< 0.4 mg m^{-3}; 75 % percentile), representative of the typical "High Nutrient Low Chlorophyll" (HNLC) conditions well reported in the Southern Ocean [70–72] (Fig. 1). The lowest values are similar to those typically observed in the most hyper-oligotrophic waters of the South Pacific [73]. The [Tchl*a*] concentrations were highest at known biological 'hotspots' within the Southern Ocean including near Subantarctic islands, Kerguelen [74,75], South Georgia-South Sandwich and Bouvet Islands [76], in the Scotia Sea [77,78], over the Patagonian shelf [79], near Mertz Glacier and within a known polynya in the MIZ of the Ross Sea and waters off the continental shelf leading to Siple

Optics EXPRESS

Island [8]. In these locations, alleviation from iron-limitation is expected to occur due to shallow bathymetry, ice-melts and deposition from the islands [67,80,81].

3.2. Very high pheopigment concentrations at high latitude

In our dataset, pheopigments (pheophorbide *a* and pheophytin *a*) make up a significant proportion of the total phytoplankton pigment concentrations, especially at latitudes in the MIZ (Fig. 3). At low latitudes 40-60°S, pheopigments were on average 10% of the [Tchl*a*], but at latitudes higher than 60°S their contribution increased drastically (up to > 100 %, mean 27 % +/- 18 %; Fig. 3). Pheopigment concentrations in the surface waters of oligotrophic ocean regions (or hyperoligotrophic ocean regions) have typically not been reported at levels higher than 5 % of [Tchl*a*] [53,54,82] (See mauve symbols in Fig. 3 from B04). The studies of Mendes et al. [83] and Wright et al. [84] which conducted North to South transects of the Indian Ocean sector of the SO both reported increasing pheopigment concentrations with increasing latitude. In Mendes et al. [83], surface concentrations of pheopigments were on average 2 % of [Tchl*a*] in subtropical waters, increasing to 12 % in antarctic waters where a maximum of 20 % was observed. Overall Wright et al. [84] observed average integrated pheopigment concentrations at 15 % of integrated [Tchl*a*]. Reynolds et al. [23] showed that pheopigment concentrations in surface waters of the PFZ and Ross Sea were strongly and linearly correlated with [Tchl*a*]. The exact formation pathway of these chlorophyll *a* degradation pigments is unclear, although in the Southern Ocean, pheophytin *a* has been linked to increased grazing pressure [83,85] and pheophorbide *a* to either grazing, cell senescence or maybe from non-living particulate matter released from nearby melting sea-ice [84].

3.3. High fraction of microplankton compared to lower latitudes for the same trophic state

Microphytoplankton (largely diatoms) increasingly dominated the phytoplankton community composition at increasing latitude (Fig. 4), even at very low chlorophyll concentrations. In our data, we did not find an overall systematic trend between community size structure and chlorophyll concentration, except above 1 mg m^{-3} where microphytoplankton made up most of the community (Fig. 4). It has previously been observed that a significant shift in phytoplankton species composition occurs at the PF which typically delineates waters of seasonal silicate limitation to the north [86]. Phytoplankton species composition in waters north of the PF, within the SAZ and PFZ, are typically more diverse, comprised of nanoeukaryotes, nanoflagellates including haptopytes, especially coccolithophores but also Phaeocystis *sp*., prasinophytes, euglenoids, cryptophytes, dinoflagellates (both autotrophic and heterotrophic), small lightly silicified diatoms, and cyanobacteria [36–38,87]. South of the PF however, diatom species typically dominate the composition with haptophytes, especially Phaeocystis *sp*., in high abundance [28,36,38,39]. Similar to Uitz et al. [10] data from the SO, the picophytoplankton fraction (f_{pico}) in our dataset never exceeded 10 % of the total pigment biomass (Fig. 5), however, cyanobacteria *Synechococcus sp.* have been reported to contribute 20 % of cell counted biomass within Northern reaches of the SAZ (via flow cytometry) [87] and as such, their low contribution to the pigment biomass may simply be due to their low chlorophyll content [88]. In Uitz et al. [10], the authors suggest that the surface layer mixing regime may help explain the contribution of (f_{micro}) to total pigment biomass. They found that in "mixed" waters of the Ross Sea (South of 60°S), i.e. where the euphotic depth was shallower than the mixed layer depth (Z_{eu}/MLD < 1), microphytoplankton dominated at low chlorophyll concentrations, and increases in chlorophyll tended to be associated with nanophytoplankton, i.e. blooms of haptophytes such as Phaeocystis *sp*. Under stratified conditions (Z_{eu}/MLD > 1) in the Ross Sea it is expected that microphytoplankton would dominate the pigment biomass based on previous observations [89–91], however, the Uitz et al. study did not include observations under those conditions. In other areas of the Southern Ocean, the

Optics EXPRESS

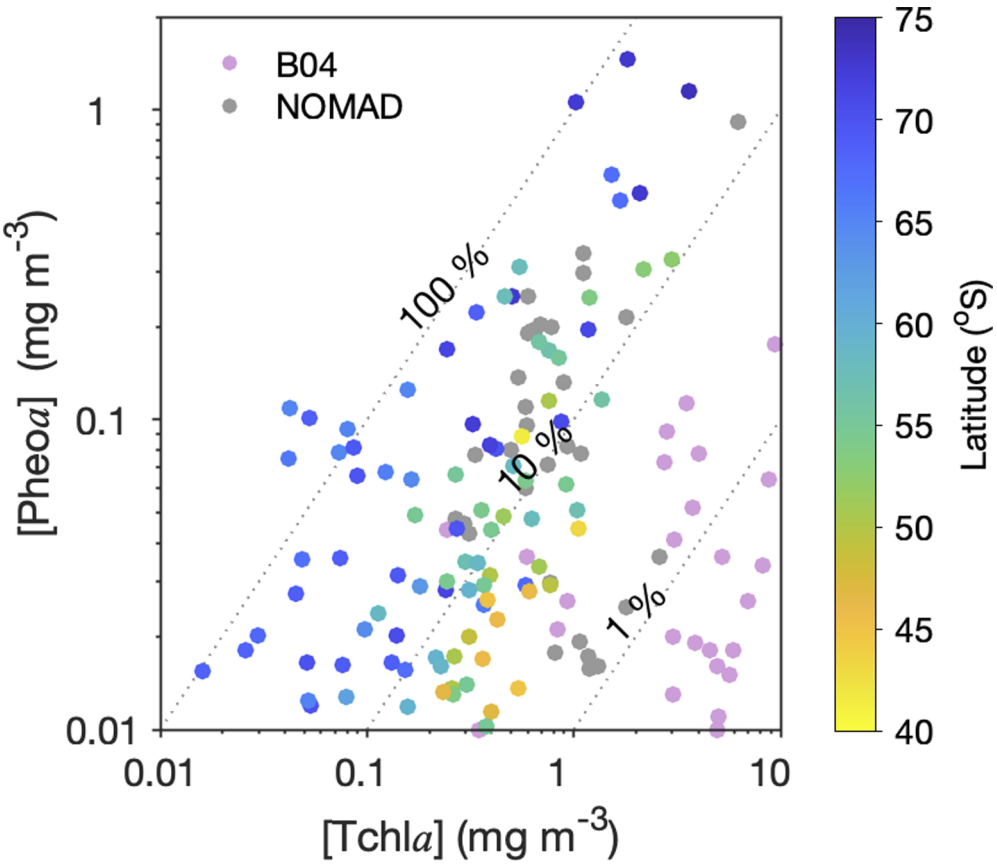

Fig. 3. Concentrations of [Pheo*a*] as a function of [Tchl*a*], colourmapped by latitude (^{o}S). Grey symbols indicate samples from NOMAD Southern Ocean subset. Mauve symbols are data from temperate oceans spanning a wide range of [Tchl*a*] from Bricaud et al. [53] (B04; most points are much lower than 1 % and do not appear on the graph). The dashed lines represent where [Pheo*a*] is 1 %, 10 % and 100 % of [Tchl*a*].

dominant species or class of phytoplankton blooms varies between haptophyte species *Phaeocystis sp.*, coccolithophores like *Emiliania huxleyi*, diatoms, and cryptophytes [92,93]. In our ACE dataset, the mixing regime alone did not explain much of the variability in microphytoplankton abundance (Fig. 4; Z_{eu}/MLD indicated by marker size), and the Z_{eu}/MLD was strongly dependent on [Tchl*a*] with the mixed vs stratified regime boundary occurring roughly at 0.2-0.3 mg m^{-3}.

3.4. *Surface [Tchla] does not relate well to the dominant phytoplankton size class*

In Uitz et al. [10], the authors presented a simple relationship between [Tchl*a*] and f_{micro} for discrete trophic (chlorophyll *a*) categories or ranges as a means to infer community composition from the surface chlorophyll *a*, which are presented in Fig. 4 overlaying our ACE dataset. In addition to the relationship parameterised for well-mixed waters of the Ross Sea (Uitz "SO Mixed"), the relationships for well-mixed waters from 60°S to 60°N (Uitz "Other Mixed"), and stratified waters from 60°S to 60°N (Uitz "Other Stratified") are also included, noting though that in Uitz et al. [10] stratified waters were not observed in the Southern Ocean. Compared to the statistics compiled by Uitz et al. [10] from 60°S to 60°N, we observed much higher proportions of microphytoplankton in the phytoplankton pigment biomass within stratified waters, especially

Optics EXPRESS

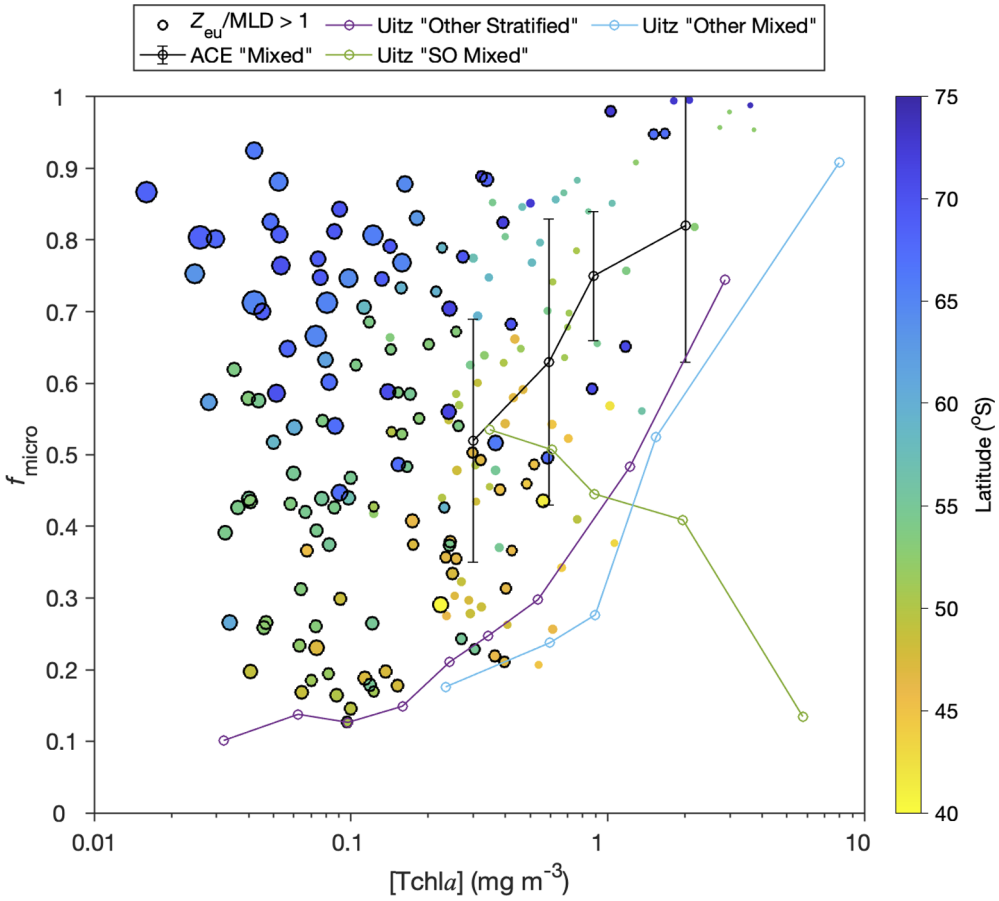

Fig. 4. Proportion of microphytoplankton (f_{micro}) as a function of [Tchl*a*] colourmapped by latitude (°S). Datapoint size indicates the mixing regime experienced by phytoplankton, Z_{eu}/MLD, see section *Physical Oceanography*. Datapoints where Z_{eu}/MLD > 1 are classed as representing 'stratified' conditions (indicated with black outer circles). Also presented on the plot are the f_{micro} vs [Tchl*a*] relationships parameterised by Uitz et al. [10], see text for details. The black lines are the parameterisation for 'mixed waters' in the ACE dataset using the same trophic categories as [10].

Optics EXPRESS

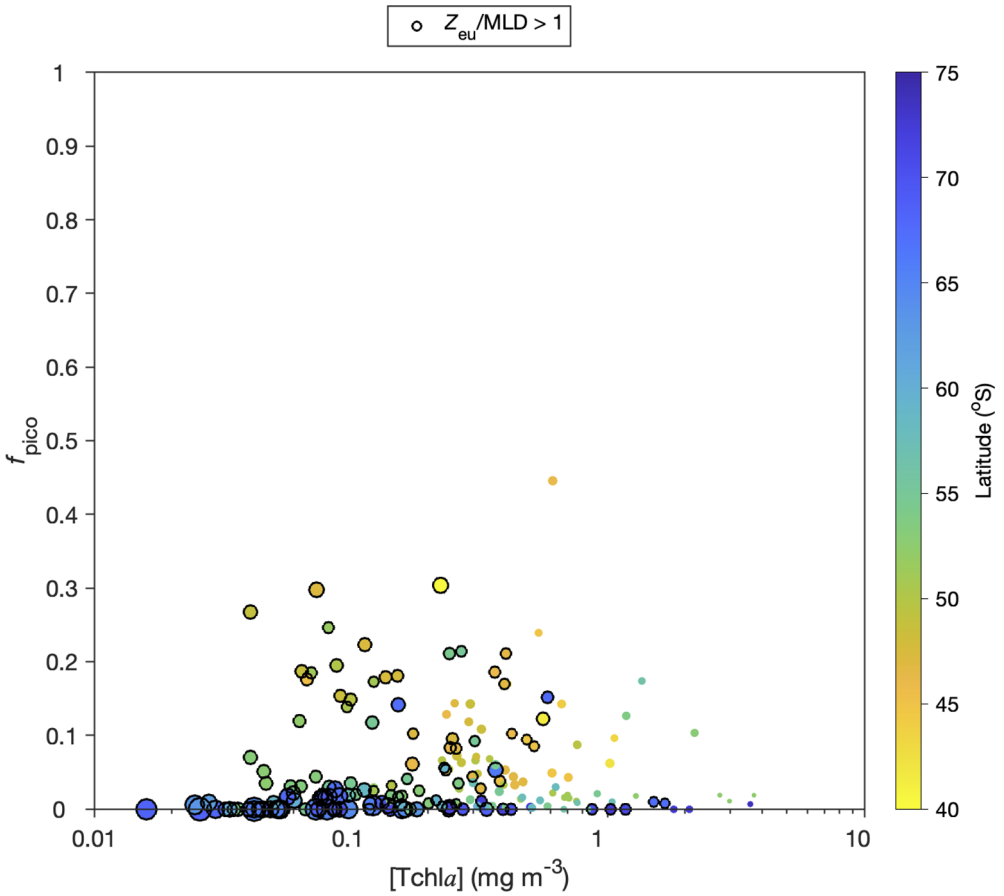

Fig. 5. Proportion of picophytoplankton (f_{pico}) as a function of [Tchl*a*] colourmapped by latitude (°S). Datapoint size indicates the mixing regime experienced by phytoplankton, Z_{eu}/MLD, see section *Physical Oceanography*.

at low [Tchl*a*]. However, the proportion of f_{micro} within each chlorophyll *a* range (see Uitz et al. [10] for the 7 stratified tropic categories) within stratified waters in the ACE dataset is highly variable, and cannot be parameterised as a function of [Tchl*a*]. In our dataset, at [Tchl*a*] between 0.2-0.8 mg m^{-3} the average f_{micro} in mixed waters is close to that observed in the equivalent trophic categories in the Uitz et al. [10] SO mixed dataset, but also highly variable. At [Tchl*a*] > 0.8, f_{micro} in our dataset continues to increase, contrary to the Uitz et al. [10] dataset. In fact at high [Tchl*a*] > 0.8, f_{micro} is much higher than all of the statistics in Uitz et al. [10]. This may be a reflection of the greater importance of diatoms to Southern Ocean phytoplankton composition relative to other oceans. Interestingly the ACE samples with high [Tchl*a*] and f_{micro} in "well-mixed" waters were sampled within the SAZ which is typically co-limited by iron and light [40,72]. These samples were predominately found on the Kerguelen Plateau (and also near Bouvetoya Island) where subsurface pools of dissolved iron on the Kerguelen Plateau within the upper 100 m were observed during ACE by Janssen et al. [94] and would be accessible to phytoplankton when waters were well mixed potentially alleviating iron limitation. However, the relationship between f_{micro} and [Tchl*a*] in "well-mixed" waters would likely change with season where during winter for example mixed layer depths can reach hundreds of metres imposing chronic light limitation on phytoplankton growth [6,95]. The high proportion of f_{micro} in stratified

Optics EXPRESS

waters south of the SACCF was unexpected, especially at such low chlorophyll *a*. These waters are often influenced by polynyas, featuring strong Phaeocystis *sp*. blooms [10,22,26], which in contrast we did not observe. We sampled the region south of the SACCF from late January to mid February and it is possible that we either observed a post-polynya bloom stage with species succession occuring from Phaeocystis *sp* to diatoms [5,8], were sampling too far off the continental shelf in waters up to 4000 m to observe the Phaeocystis *sp* dominated waters [8], or that the dissolved iron had been depleted below levels required by Phaeocystis *sp*, which can have a higher iron requirement than diatoms [96]. Similar to our study, the study by Hewes [97] in waters south of the ACC identified a low chlorophyll *a* scenario where phytoplankton in low-iron conditions in shoaled waters were dominated by microphytoplankton. Although Z_{eu}/MLD was derived using a climatological MLD, this is not biasing the relationships between f_{micro} and [Tchl*a*]. We observed the same trends in [Tchl*a*] vs f_{micro} in a smaller sample set of n=28 using MLDs calculated from CTD density profiles, and corresponding pigment samples collected using niskin bottles on the same casts at surface depths < 10 m (data not shown). It is clear from this ACE dataset that the paradigm of phytoplankton size class increasing and decreasing proportionally with phytoplankton biomass (e.g., chlorophyll *a* concentration) [98,99], does not always apply to the SO, and as we show below has implications for the interpretation of bio-optical properties.

3.5. Particle volume increases with latitude for a given [Tchla]

The relationship between [Tchl*a*] and particle volume varies between high and low latitude waters in the Southern Ocean. In latitudes south of 60°S, increases in [Tchl*a*] are strongly associated with an increase in the total particle volume [Total particle volume=3.2×10^{10}[Tchl*a*]$^{0.97}$, R^2 0.76; see power law relationships in Fig. 6(a)] as well as an increase in the mean equivalent spherical particle volume [or size; Mean particle volume=141[Tchl*a*]$^{0.42}$, R^2 0.72; see section *Particle Size Distribution* and Fig. 6(b)]. At latitudes 50-60°S, total particle volume is less strongly related to increases in [Tchl*a*] (Total particle volume=4.1×10^{9}[Tchl*a*]$^{0.53}$, R^2 0.43). The mean particle volume also appears to be less variable and overall smaller in size [Mean particle volume=60.9[Tchl*a*]$^{0.33}$, R^2 0.33; Fig. 6(b)]. At lower latitudes 40-50°S total particle volume and mean particle volume show no apparent increase with [Tchl*a*] [R^2 of both relationships close to 0 and p>0.05; see Figs. 6(a) and 6(b)]. It is however difficult to fully interpret these trends as non-phytoplankton particles are also counted here and as shown earlier, pheopigment concentrations, and hence degraded or detrital particles are important components of the particulate matter. It is possible though that in the northern reaches of the SAZ, changes in chlorophyll *a* were manifested as adjustments in chlorophyll *a* per cell which could be an acclimation response to low dissolved iron concentrations or photoacclimation to changes in the mixing layer depth [100–102].

3.6. Particulate absorption is tightly linked to [Tchla] with significant background of non-algal particles

The particulate absorption coefficient at 440 nm (a_p(440), m^{-1}) in the ACE and NOMAD datasets increased with [Tchl*a*] in a similar manner to B04 [53] and B98 [64] [Fig. 7(a); Table 1], but was systematically lower than B04 [53] at [Tchl*a*] > 0.1 mg m^{-3}. Overall there was little variance in the relationship at any given [Tchl*a*]. The coefficient and exponent for the a_p(440) vs. [Tchl*a*] was a_p(440)=0.043[Tchl*a*]$^{0.61}$ (R^2=0.89; Table 1). The slope is similar to Reynolds et al. [23] for data for the Ross Sea (0.041) and PFZ (0.047), and the NOMAD dataset (0.044) from Drake's Passage, Scotia Sea and Antarctic Peninsula waters. It is also in agreement with previous observations that chlorophyll-specific particulate absorption a_p^* is generally lower in the Southern Ocean [18,23] than values reported for other oceans. Lower slopes in the relationship between a_p(440) and [Tchl*a*] imply that a lower increase in absorption per unit [Tchl*a*], or lower a_p^*. Lower values of a_p^* per unit chlorophyll *a* may result from smaller contributions to particulate absorption by

Optics EXPRESS

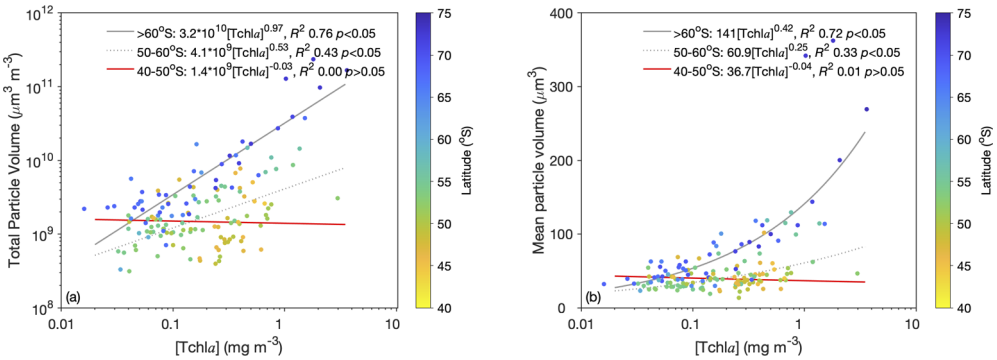

Fig. 6. (a) The total particle volume (μm m^{-3}) of samples as a function of [Tchl$a$]. (b) The mean (equivalent spherical) particle volume (μm^3) as a function of [Tchl$a$]. Data points in a) and b) are colour mapped by latitude (°S).

a_{nap}, reduced contributions by pigments other than chlorophyll a to phytoplankton absorption, or variability in absorption per unit chlorophyll a resulting from pigment packaging effects [103]. An interesting feature in Fig. 7(a) is the change of slope of $a_p(440)$ at low [Tchl$a$] (at around $a_p(440)$ = 0.006 m^{-1} and 0.1 mg m^{-3} [Tchl$a$]) that may arise from an increased proportions of non-algal particles (e.g., heterotrophic bacteria, detritus, viruses, minerogenic particles; see also Fig. 16). This is reminiscent of the relationship between particulate backscattering and chlorophyll a seen in Brewin et al. [104] which was attributed to an increased background of non-algal particles and the observation by Zhang et al. [105] of a significant background signal from sub-micron particles in the particulate backscattering in low chlorophyll a waters of the North Pacific which become a more important part of the signal at low chlorophyll a compared to at high chlorophyll a.

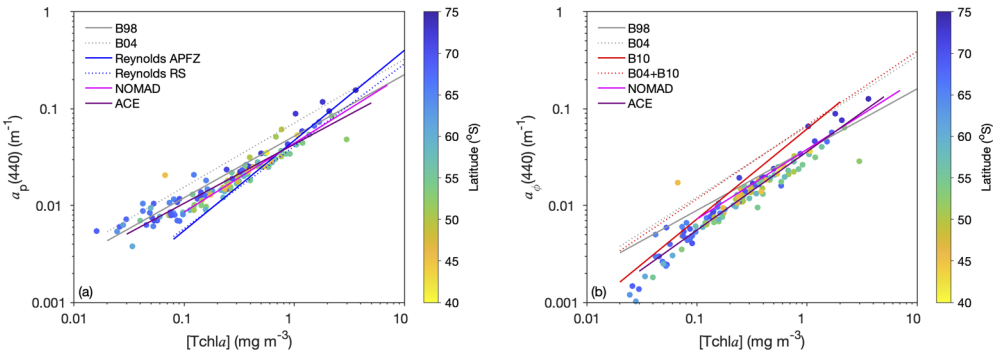

Fig. 7. Variations in (a) particulate absorption [$a_p(440)$] and (b) phytoplankton absorption ($a_\phi(440)$) at 440 nm as a function of [Tchl$a$]. Purple line indicates parameterised ACE data relationships. Magenta line indicates relationship from the NOMAD dataset. Previously parameterised relationships of B98 [64] (solid grey line), B04 [53] (dashed grey line), B10 [54] (solid red line), B10+B04 [53,54] combined datasets (our fit to combined original datasets; dashed red line), Reynolds et al. [23] in the APFZ (solid blue line) and Ross Sea (dashed blue line) are also plotted.

Optics EXPRESS

Table 1. Constants and Exponents From the Power Law Relationships Between Chlorophyll *a* (either [Tchl*a*] or [Tchl*a*+Pheo*a*]) and a) $a_p(440)$, b) $a_\phi(440)$, or c) $a_\phi(676)$ from the ACE dataset (ACE), B98 [64], B04 [53], B10 [54], B04+B10 [53,54] Combined Datasets (our fit to combined original datasets; dashed red line), and Reynolds et al. [23] in the APFZ (RAPFZ) and Ross Sea (RRS).[a]

a) Study	$a_p(440)$=Const[Tchl$a$]^{exp}	$a_p(440)$=Const[Tchl$a$+Pheo$a$]^{exp}
ACE	$a_p(440)=0.043[\text{Tchl}a]^{0.61}$	-
B98	-	$a_p(440)=0.052[\text{Tchl}a+\text{Pheo}a]^{0.64a}$
B04	-	$a_p(440)=0.071[\text{Tchl}a+\text{Pheo}a]^{0.66a}$
RAPFZ	$a_p(440)=0.047[\text{Tchl}a]^{0.93}$	-
RRS	$a_p(440)=0.041[\text{Tchl}a]^{0.85}$	-
NOMAD	$a_p(440)=0.44[\text{Tchl}a]^{0.71}$	-
b) Study	$a_\phi(440)$=Const[Tchl$a$]^{exp}	$a_\phi(440)$=Const[Tchl$a$+Pheo$a$]^{exp}
ACE	$a_\phi(440)=0.036[\text{Tchl}a]^{0.81}$	$a_\phi(440)=0.032[\text{Tchl}a+\text{Pheo}a]^{0.84}$
B98	-	$a_\phi(440)=0.038[\text{Tchl}a+\text{Pheo}a]^{0.63a}$
B04	-	$a_\phi(440)=0.065[\text{Tchl}a+\text{Pheo}a]^{0.73a}$
B10	-	$a_\phi(440)=0.062[\text{Tchl}a+\text{Pheo}a]^{0.93a}$
B04+B10	-	$a_\phi(440)=0.067[\text{Tchl}a+\text{Pheo}a]^{0.76a}$
NOMAD	$a_\phi(440)=0.038[\text{Tchl}a]^{0.72}$	$a_\phi(440)=0.035[\text{Tchl}a+\text{Pheo}a]^{0.72}$
c) Study	$a_\phi(676)$=Const[Tchl$a$]^{exp}	$a_\phi(676)$=Const[Tchl$a$+Pheo$a$]^{exp}
ACE	$a_\phi(676)=0.020[\text{Tchl}a]^{0.82}$	$a_\phi(676)=0.018[\text{Tchl}a+\text{Pheo}a]^{0.87}$
B98	-	$a_\phi(676)=0.018[\text{Tchl}a+\text{Pheo}a]^{0.82a}$
B04	-	$a_\phi(676)=0.026[\text{Tchl}a+\text{Pheo}a]^{0.89a}$
B04+B10	-	$a_\phi(676)=0.026[\text{Tchl}a+\text{Pheo}a]^{0.93a}$
NOMAD	$a_\phi(676)=0.017[\text{Tchl}a]^{0.82}$	$a_\phi(676)=0.016[\text{Tchl}a+\text{Pheo}a]^{0.83}$

[a]Note that for B98, B04, B10, and B04+B10 that pheopigments contributed less than 5% to the [Tchl*a*+Pheo*a*].

3.7. *Phytoplankton absorption is lower than in other oceans for the same [Tchla]*

The phytoplankton absorption coefficient at 440 nm [$a_\phi(440)$] as a function of [Tchl*a*] [Fig. 7(b); Table 1] reflects the absorption by all photosynthetic and non-photosynthetic pigments in this waveband. It was 50% lower than the relationship derived by B04 [53] for the first optical depth in tropical and temperate oceans and seas (ACE data $a_\phi(440)=0.036[\text{Tchl}a]^{0.82}$ R^2=0.91). At [Tchl*a*] greater than 0.1 mg m^{-3} that ACE values were more similar to the NOMAD dataset and at >0.3 mg m^{-3} the ACE values $a_\phi(440)$ are more similar to the B98 [64] dataset, which included data from all depths up to 200 m (i.e., greater than 1 optical depth) where samples are strongly impacted by pigment packaging and hence substantially lower than the B04 [53] coefficients. As the exponent for the ACE data suggests, the relationship is non-linear, and at [Tchl*a*] below 0.3 mg m^{-3} $a_\phi(440)$ is even lower and were more similar (though still lower) to those measured in the ultra oligotrophic waters of the south-east Pacific as reported in B10 [54].

Absorption by phytoplankton at 676 nm is predominantly due to chlorophyll *a* pigments, and so changes to the chlorophyll-specific absorption coefficient at 676 nm are generally mostly due to changes in pigment packaging only, rather than adjustments in carotenoid pigments from changes to the community composition and/or the photophysiological (pigment) response. The chlorophyll-specific absorption coefficient at 676 nm ($a^*_\phi(676)$) normalised to [Tchl*a*] was on average 0.020 m^2 mg^{-1} [Fig. 8(a); Table 1], similar to the *in vivo* specific absorption coefficient for unpackaged chlorophyll *a* of Bricaud et al. [82] (0.0207 m^2 mg^{-1}), Bidigare et al. [62] (0.0199

Optics EXPRESS

m^2 mg^{-1}) and Clementson and Wojtasiewicz [59] (0.0196 m^2 mg^{-1}). However, $a^*_\phi(676)$ declined with [Tchl*a*] ($a^*_\phi(676)=0.020[\text{Tchl}a]^{0.82-1}$) [and with increasing cell volume, see Fig. 8(b)], and was substantially lower than the B04 [53] and B04+B10 [54] relationships at Tchl*a*] > 0.1, suggesting that this ACE dataset is more packaged than observed in other temperate and tropical oceans. The $a^*_\phi(676)$ was most similar to the NOMAD data from the SO, and B98 [64] data from temperate and tropical oceans which has also been described as being impacted by packaging. Comparing Figs. 8(a) and 8(b) (which has been normalised to [Tchl*a* + Pheo*a*]), there is noticeable scatter of $a^*_\phi(676)$ in Fig. 8(a) that is absent in Fig. 8(b), which is attributable to increased absorption by pheopigments in samples with high [Pheo*a*/Tchl*a*] at high latitudes [see colourmap of Fig. 8(a)]. Although the overall relationship of $a^*_\phi(676)$ (normalised to [Pheo*a*/Tchl*a*]) vs [Pheo*a*/Tchl*a*] is not different to the relationship above, $a^*_\phi(676)=0.018[\text{Tchl}a + \text{Pheo}a]^{0.87-1}$ [CE relationship from Fig. 8(b); Table 1], it is clear that on a case by case basis, pheopigments may contribute substantially to $a_\phi(676)$ and cannot be discounted as being an important part of the optical constituents in the Southern Ocean, especially at high latitudes. As seen in Fig. 9(a), $Q^*_a(676)$ coefficient decreases in value with increasing [Tchl*a*] and increasing cell volume, confirming increased pigment packaging with increasing [Tchl*a*] due to increasing cell size and increased intracellular chlorophyll content. By definition, Q^*_a should range from 1 to 0, and values > 1 as seen in Fig. 9(a) indicate the phytoplankton absorption is greater than that of the same pigment material in solution [103]. Other studies have observed Q^*_a > 1 [53,106–108] and have attributed this to missing pigments (e.g., phycobilins) or other light absorbing compounds not detectable by HPLC [109], cellular components and structure such as thylakoid stacking which contribute to a_ϕ [108], differences in *in vivo* absorption vs absorption by pigments in solution which may be due to pigment complex construction or is unexplained [110], and/or natural or species-specific variability in the weight-specific pigment absorption coefficients [110]. It is not clear which explanation is responsible for the discrepancies in this dataset, and as mentioned in the section *Pigment and Packaging Indices*, the a_{miss} term solution of Bricaud et al. [53] did not seem to be correct for our dataset. Nevertheless, the general trends in Q^*_a (regardless of the absolute magnitude) as a function of [Tchl*a*] and cell volume are as expected.

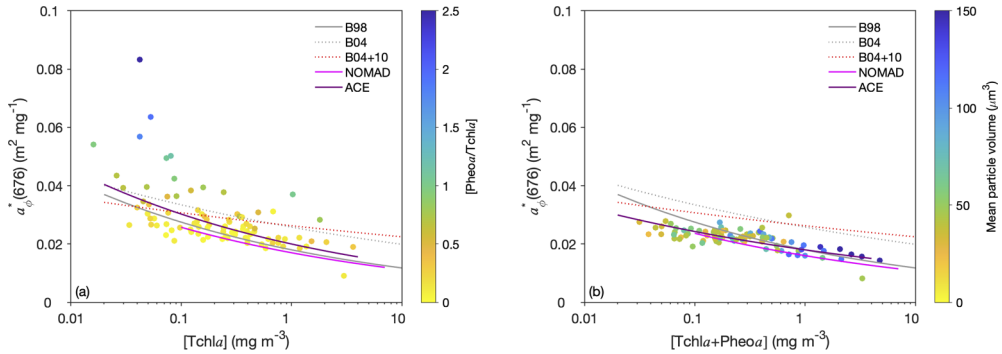

Fig. 8. Variations in chlorophyll-specific *a* phytoplankton absorption at 676 nm ($a^*_\phi(676)$). (a) $a^*_\phi(676)$ is normalised to and plotted as a function of [Tchl*a*], and colour mapped by [Pheo*a*/Tchl*a*]. (b) $a^*_\phi(676)$ is normalised to and plotted as a function of [Tchl*a* + Pheo*a*] as a function of [Tchl*a* + Pheo*a*], and colourmapped by mean particle volume (μm^3). Purple line is the ACE dataset parameterisation. Magenta line is the NOMAD dataset parameterisation. Previously parameterised relationships of B98 [64] (solid grey line), B04 [53] (dashed grey line), and B04+B10 [53,54] combined datasets (our fit to combined original datasets; dashed red line) are also plotted.

Optics EXPRESS

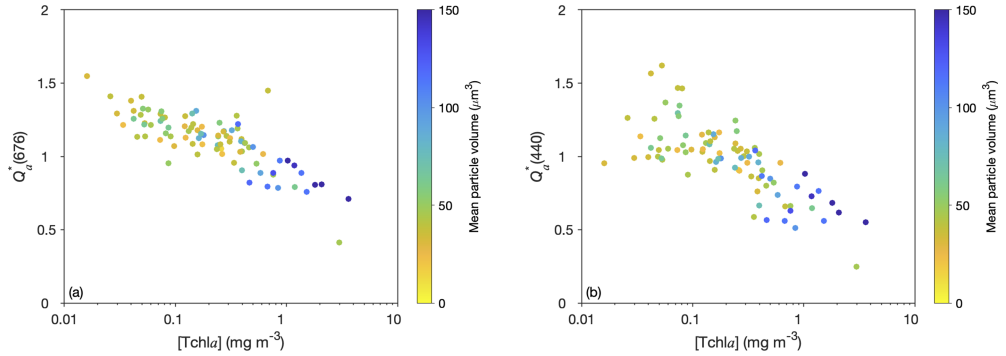

Fig. 9. Packaging indices calculated at (a) 440 nm ($Q_a^*(440)$) and (b) 676 nm ($Q_a^*(676)$) using the pigment reconstruction method, plotted as a function of [Tchl$a$]. Both (a) and (b) are colourmapped by mean particle volume (μm^3).

Very low $a_\phi^*(440)$ at chlorophyll a concentrations below 0.3 mg m^{-3} were observed compared to previously described fits from temperate and tropical oceans [Fig. 10(a)] and also the SO (i.e., NOMAD). However, in the ACE dataset, although values of $a_\phi^*(440)$ measured on samples with > 0.3 mg m^{-3} chlorophyll a still depart strongly from global surface waters values of B04 and B04+10 [53,54,64] they more closely resembles values that include deeper waters from B98 [64] and NOMAD SO data. Chlorophyll-specific absorption at 440 nm is typically lower in microphytoplankton [31]. This is clearly illustrated in this dataset which is dominated by microphytoplankton (Fig. 5). The $a_\phi^*(440)$ is also impacted by changes in the concentration of accessory pigments which overlap with chlorophyll a absorption at 440 nm. According to $a_\phi^*(440)$ vs. [Tchl$a$] relationships parameterised in non-polar waters, $a_\phi^*(440)$ is typically much higher at low chlorophyll accounting for the predominance of picophytoplankton when chlorophyll is low in temperate and tropical waters. Pigment packaging at 440 nm does appear to explain the trends in $a_\phi^*(440)$ within the ACE dataset, similar to $Q_a^*(676)$, $Q_a^*(440)$ also decreases with [Tchl$a$] and cell volume [Fig. 9(b)], as has been observed by others [18]. However, it does not appear to fully explain why $a_\phi^*(440)$ is so much lower than observations in temperate and tropical oceans and varies so little with [Tchl$a$] compared to previously described trendlines. Unlike at 676 nm, pheopigments do not contribute substantially to absorption at 440 nm (Fig. S1 in Supplement 1), and so there is a smaller difference between Figs. 10(a) and 10(b), where Fig. 10(b) has been normalised to [Tchl$a$ + Pheo$a$].

Figures 11(a) and 11(b) show $a_\phi^*(440)$ and $a_\phi^*(676)$, respectively, as a function of the median light intensity within the mixed layer (I_g). Overall, there is very little change in the chlorophyll-specific absorption coefficient at 440 or 676 with increases in I_g except at I_g > 200. This suggests that variation in $a_\phi^*(440)$ and $a_\phi^*(676)$ in this dataset are due to changes in cell size and pigmentation driven by changes in taxa. It is noted though that when surveying bio-optical properties in surface waters, i.e., across the horizontal dimension, the dominant source of variation in a_ϕ^* tends to be changes in the phytoplankton size structure and pigment composition from changes in taxa, as opposed to the vertical dimension where photoacclimation become more important [111].

3.8. *High photosynthetic and [Tchlc] together with low photoprotective and [Tchlb] pigments complement characterise the Southern Ocean in summer*

Bricaud and coauthors [54] (B10) surveyed the ultra-oligotrophic waters of the South-Pacific gyre and found that for low chlorophyll samples $a_\phi(440)$ (and hence $a_\phi^*(440)$) were 30%-40% lower than in other oceanic areas with the same chlorophyll. They attributed this to both a

Optics EXPRESS

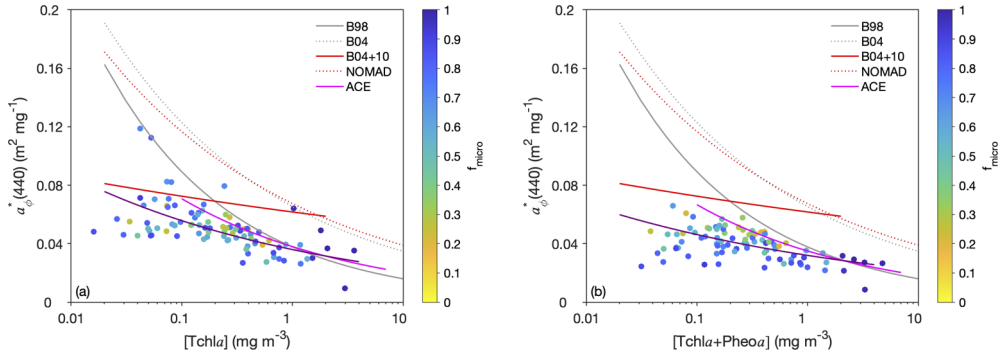

Fig. 10. Variations in chlorophyll-specific a phytoplankton absorption at 440 nm ($a^*_\phi(440)$). (a) $a^*_\phi(440)$ is normalised to and plotted as a function of [Tchl$a$], and colourmapped by [Pheo$a$/Tchl$a$]. (b) $a^*_\phi(440)$ is normalised to and plotted as a function of [Tchl$a$ + Pheo$a$] as a function of [Tchl$a$ + Pheo$a$], and colourmapped by f_{micro}. Purple line is the ACE dataset parameterisation. Magenta line is the NOMAD dataset parameterisation. Previously parameterised relationships of B98 [64] (solid grey line), B04 [53] (dashed grey line), and B04+B10 [53,54] combined datasets (our fit to combined original datasets; dashed red line) are also plotted.

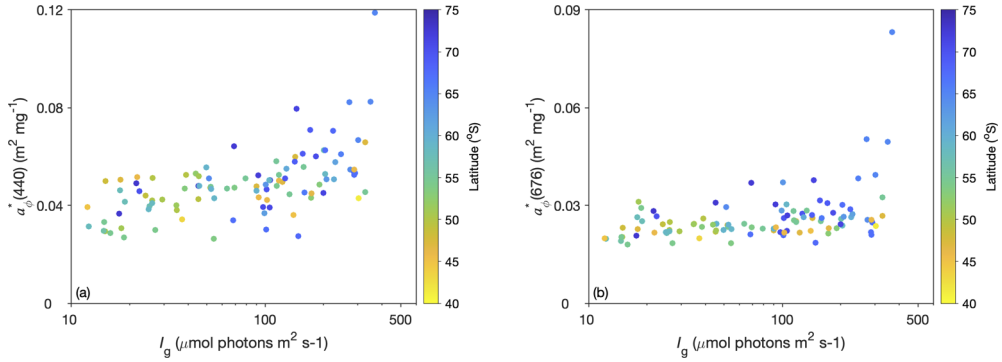

Fig. 11. Chlorophyll-specific a phytoplankton absorption at (a) 440 nm ($a^*_\phi(440)$) and (b) 676 nm ($a^*_\phi(676)$) as a function of the median light intensity within the mixed layer (I_g), colourmapped by latitude (°S). Note the different scale in (b).

decrease in the concentration of accessory pigments, specifically photoprotective carotenoids, relative to chlorophyll a ([PPC/Tchl$a$], and an increase in relative cell size. In the ACE dataset, the relative contribution of two of the major pigment groups, [Tchl$b$] [Fig. 12(a)] and [PPC] [Fig. 12(d)] are generally lower (compare mauve and ACE points in Fig. 12) for the same [Tchl$a$] than in other oceans. In addition to the lower growth irradiance compared to other oceans, this likely due to the lower contribution of picophytoplankton to the Southern Ocean pigment biomass specifically chlorophytes and cyanobacteria which contain significant concentrations of chlorophyll b, zeaxanthin, lutein and violaxanthin. High chlorophyll c and [PSC] concentrations are due to the dominance of diatoms, haptophytes and dinoflagellates [Fig. 12(b)].

It should be noted that in the Southern Ocean literature, the relationship between a_ϕ and [Tchl$a$] varies widely. For example $a_\phi(440)$ vs. [Tchl$a$] measured by Clementson et al. [20] in the Indian Ocean Sector of the SAZ in late summer were similar to the relationship of B04 [53]. In other studies, considerable variation has been observed within a single study, for example

Optics EXPRESS

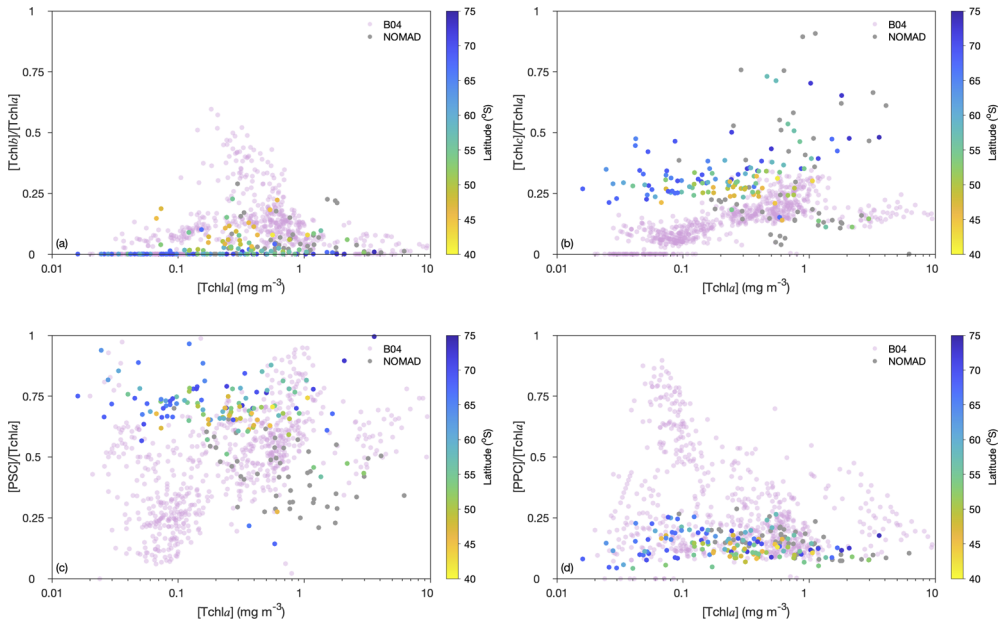

Fig. 12. Ratios of major accessory and degradation pigments to [Tchl*a*], including (a) [Tchl*b*], (b) [Tchl*c*], c) [PSC], d) [PPC]. Grey symbols indicate samples from NOMAD Southern Ocean subset. Mauve symbols are data from Bricaud et al. [53]. In (b) we note the highly variable and sometimes very high [Tchl*c*] / [Tchl*a*] in the NOMAD dataset which may be artefactual.

Kerkar et al. [25] also observed the Indian Ocean sector of the SAZ in summer and reported chlorophyll-specific $a^*_\phi(440)$ ranging from 0.04-0.5 for fluorometrically derived chlorophyll *a* between 0.11-0.26. We have also observed a large variation in $a^*_\phi(440$ nm) with very little change in [Tchl*a*] in the Atlantic and Indian Ocean sectors during the austral winter (data unpublished). Although it is acknowledged that methodological differences in the measurement (fluorometric vs. HPLC) and definition of chlorophyll *a*, application of integrating spheres for measuring optical density, pathlength amplification factors for calculating a_p and method for decomposing a_p and a_ϕ add uncertainties and variability to these measurements and relationships. We have limited these potential discrepancies in our comparison with the Bricaud datasets by: (1) running the HPLC samples in the same laboratory, (2) using both the [Tchl*a*] and [Tchl*a* + Pheo*a*] normalization approach, (3) verifying that the decomposition approach provided consistent results at 440 and 676 nm with the Bricaud and Stramski [112] approach used in some of campaigns of the Bricaud datasets. Both the inversion method presented here, and the Bricaud & Stramski approach produced reliable estimates of a_ϕ as compared to a small number of values from ACE derived using the traditional methanol extraction method of Kishino et al. [113]. For absorption measurements, some of the difference could arise from the measurement methods used such as using an integrating sphere with associated path-length amplification approach in our case. The use of an integrating sphere reduces the measurement error as more scattered photons are captured in the detector than other techniques (e.g., transmittance and transmittance-reflectance) [114] and path-length amplification factors for the integrating sphere technique have lower uncertainties than the other techniques [114,115]. However, as more scattered photons are captured by the detector, rather than be attributed to absorption, a_p could theoretically be lower when using this method as compared to others.

Optics EXPRESS

3.9. Flatter absorption spectrum and lower a^*_ϕ across the spectrum compared to other oceanic regions

The low chlorophyll-specific absorption coefficients are associated with a significant flattening of the phytoplankton absorption spectral shape as observed in the ratio $a_\phi(440)/a_\phi(676)$ (Fig. 13). In other oceanic regions $a_\phi(440)/a_\phi(676)$ increases strongly with decreasing chlorophyll a as pigment packaging decreases due to decreasing cell size, and picophytoplankton dominate (See B98, B04, B04+10 and NOMAD relationships in Fig. 13). As we show, such changes in the phytoplankton size distribution are not present in the same way in the Southern Ocean (Figs. 4 and 5). While there is a slight increase in the $a_\phi(440)/a_\phi(676)$ with decreasing [Tchl$a$] at lower latitudes, this is not observed at higher latitudes (Fig. 13). To represent these unique relationships, different spectral models are needed. Power law functions between log-transformed $a_\phi(\lambda)$ and log-transformed [Tchl$a$] were fit at 2 nm wavelength intervals (see Data File 1, Data File 2, and Data File 3 and Supplement 1 for coefficients). The resulting phytoplankton absorption spectral shapes normalized to $a_\phi(440)$ (Fig. 14), and their chlorophyll-specific equivalents (Fig. 15), show very different shapes and amplitudes compared to other oceanic regions. The equivalent shapes from the combined datasets of B04 [53] and B10 [54] are in mauve in Figs. 14(a) and Fig. 15(a). Overall the spectral shapes are noticeably different from the B04+B10 shapes, but

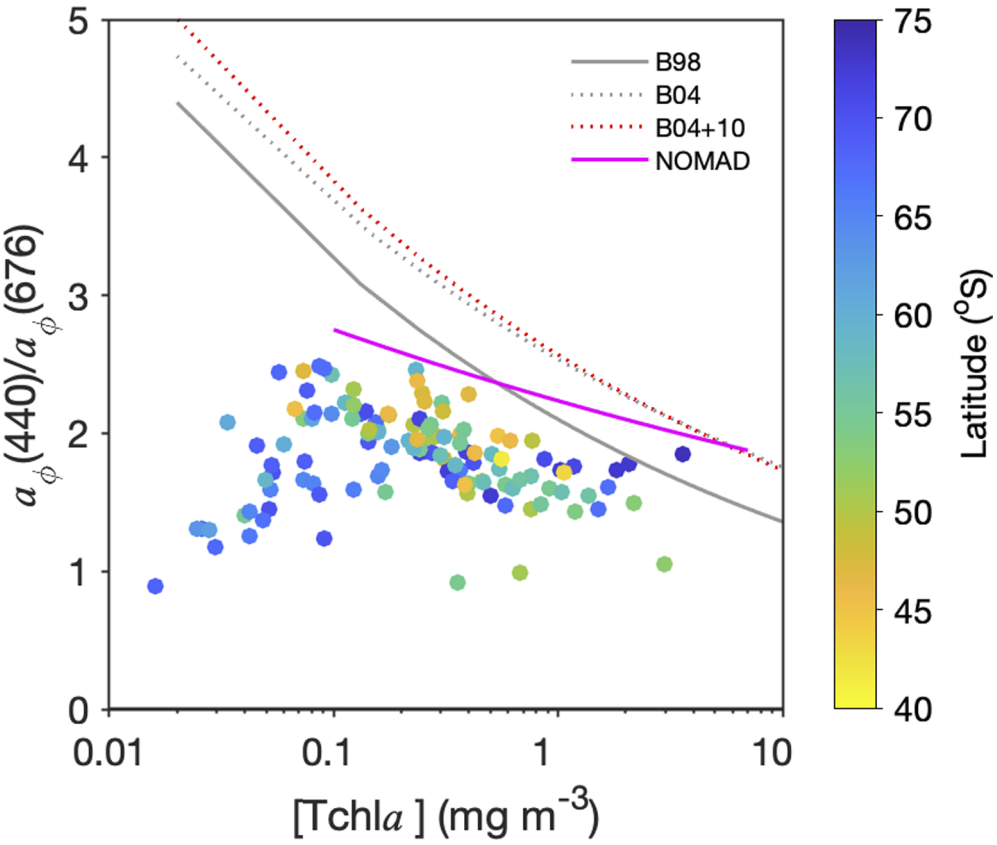

Fig. 13. Ratio of $a_\phi(440)/a_\phi(676)$ as a function of [Tchl$a$]. Previously parameterised relationships of B98 [64] (solid grey line), B04 [53] (dashed grey line), and B10 [54] (solid red line) and B04+B10 [53,54] combined datasets (dashed red line) are also plotted. The relationship from the NOMAD dataset is indicated by the magenta line.

Optics EXPRESS

differ again between low and high latitudes [Figs. 14(b), 14(c), 15(b), and 15(c)]. The shape and magnitude of the absorption spectra for phytoplankton reflect the pigment composition and concentration, which are in turn dictated by the species composition, size and environment. In addition to the higher values above ~ 500 nm reflecting the flatter, more packaged spectra, the most prominent feature in the ACE spectral shapes are a shoulder at 460 nm and between 550-600 nm which intensify at low chlorophyll *a* concentrations. The spectral peak at 460 nm is likely due to increased chlorophyll *c*, a diagnostic pigment marker for diatoms. Similar spectral features between 550-600 nm have been observed in haptophytes (e.g., Phaeocystis *sp.*) and nanoeukaryotes of the ultraplankton (2-5 μm) or nanophytoplankton (5-20 μm) size [28,31]. Also different to the average global spectral shapes is the variability at 676 nm. In the high latitude samples [Figs. 14(c) and 15(c)] the spectral shapes are more similar to a microphytoplankton shape across all chlorophyll *a* concentrations [31], including features at 460 nm (where absorption at 460 nm is lower than 440 nm) and 500 nm due to chlorophyll *c* pigments and fucoxanthin pigments. There is also very little change in the $a_\phi(440)/a_\phi(676)$ with chlorophyll *a* concentration. Whereas, in the low latitude samples, there appears to be a more significant taxonomic shift from high chlorophyll *a* to low chlorophyll *a* concentrations. These differences are particularly important when examining the chlorophyll-specific absorption. In most oceanic waters [see mauve lines in Fig. 15(a)], the chlorophyll-specific absorption does not change much above ~ 540 nm when chlorophyll *a* concentration changes, while the shorter wavelengths increase rapidly with decreasing chlorophyll *a* concentration reaching as high as ~ 0.16 m^2 mg^{-1} at ~ 450 nm. In the Southern Ocean, a_ϕ^* increases with decreasing chlorophyll *a* concentration at all wavelength,

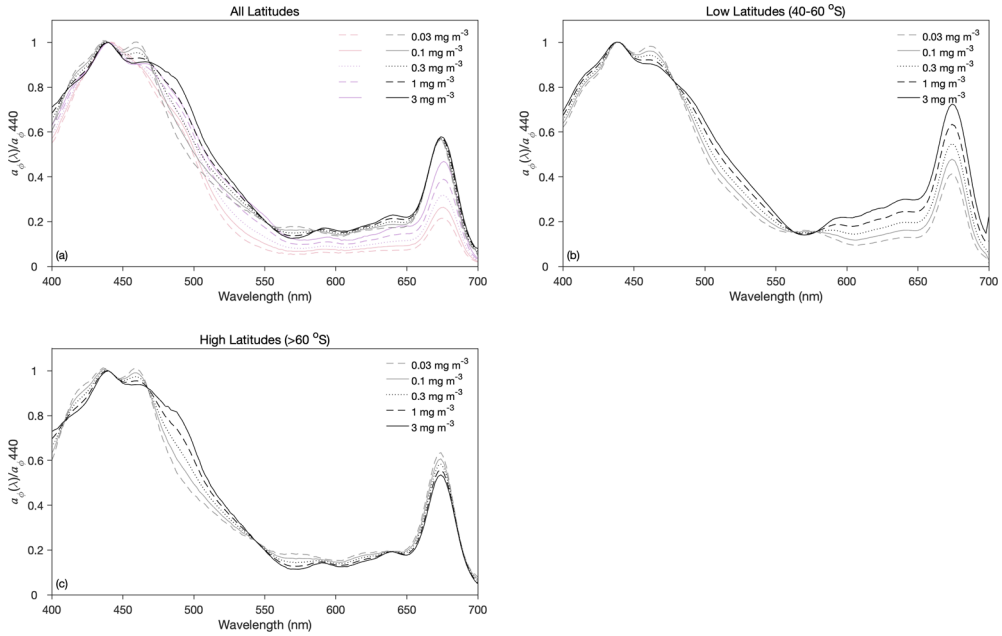

Fig. 14. Phytoplankton absorption $a_\phi(\lambda)$ spectra normalised to $a_\phi(440)$ for various values of [Tchl*a*] from the ACE dataset. The $a_\phi(\lambda)$ have been reconstructed using constants and exponents from power law functions fitted between log-transformed $a_\phi(\lambda)$ and log-transformed [Tchl*a*] at for each wavelength 400-700 nm at 2 nm wavelength intervals. The functions were fitted for (a) all latitudes, (b) low latitudes between 40 to 60°S, and (c) high latitudes southwards of 60°S. The $a_\phi(\lambda)/a_\phi(440)$ from the power law functions of the combined B04+B10 [53,54] datasets are presented in (a) as mauve lines.

Optics EXPRESS

but much less than in other oceans, reaching ~ 0.08 m^2 mg^{-1} in the low latitude waters and about half of that in higher latitudes. Similarly, at 3 mg m^{-3} of chlorophyll *a* the a^*_ϕ is about half of the a^*_ϕ in other oceanic regions. The implication of these changes are important. From an ecological perspective, phytoplankton in the Southern Ocean exhibit higher pigment packaging implying that they must invest more energy into pigment synthesis. From a remote sensing perspective, the absorption in the blue band specific to phytoplankton is significantly lower (a half to a quarter) when compared to other oceanic regions.

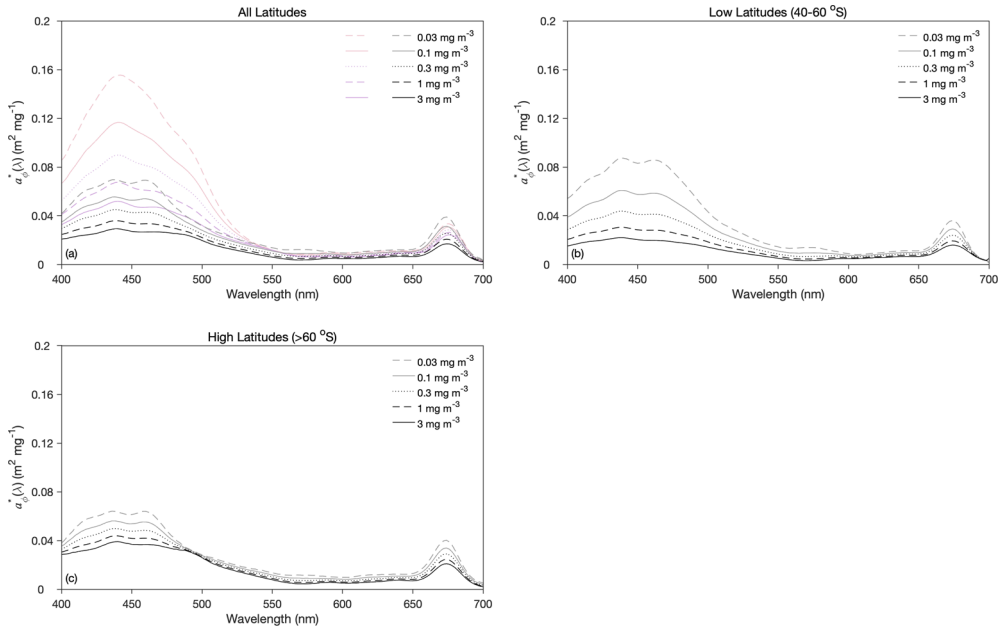

Fig. 15. Chlorophyll-specific phytoplankton absorption $a^*_\phi(\lambda)$ spectra for various values of [Tchl*a*] from the ACE dataset. The $a^*_\phi(\lambda)$ have been reconstructed using constants and exponents from power law functions fitted between log-transformed $a^*_\phi(\lambda)$ and log-transformed [Tchl*a*] at for each wavelength 400-700 nm at 2 nm wavelength intervals. The functions were fitted for (a) all latitudes, (b) low latitudes between 40 to 60°S, and (c) high latitudes southwards of 60°S. The $a^*_\phi(\lambda)$ from the power law functions of the combined B04+B10 [53,54] datasets are presented in a) as mauve lines.

3.10. Southern Ocean has high non-algal particulate absorption compared to other oceanic regions

Given the difference in relationship between $a_\phi(440)$ and [Tchl*a*] [Fig. 7(b)], relative to changes in $a_p(440)$ and [Tchl*a*] [Fig. 7(a)] (particularly at low chlorophyll *a*), it is clear that the contribution of non-algal particulates ($a_{nap}(440)$) to the total particulate absorption budget must also deviate from expected relationships. Previous reports suggest that a_{nap} contributes little to total particulate absorption in the Southern Ocean, except at locations close to landmasses or ice-shelves and is strongly related to chlorophyll *a* [18,20,23]. In contrast we find that a_{nap} can be responsible for up to 85% of particulate absorption, varying loosely in an inverse manner with phytoplankton biomass [Tchl*a*] (Fig. 16). Overall the contribution is considerably higher than observed in temperate oceans at comparable chlorophyll *a* (See data from B04 [53] in Fig. 16). This is especially true in high latitude waters where increased pheopigment concentrations (Figs. 3

Optics EXPRESS

and 16) suggests that phytoplankton biomass is increasingly degraded and redistributed to the non-algal particulate pool.

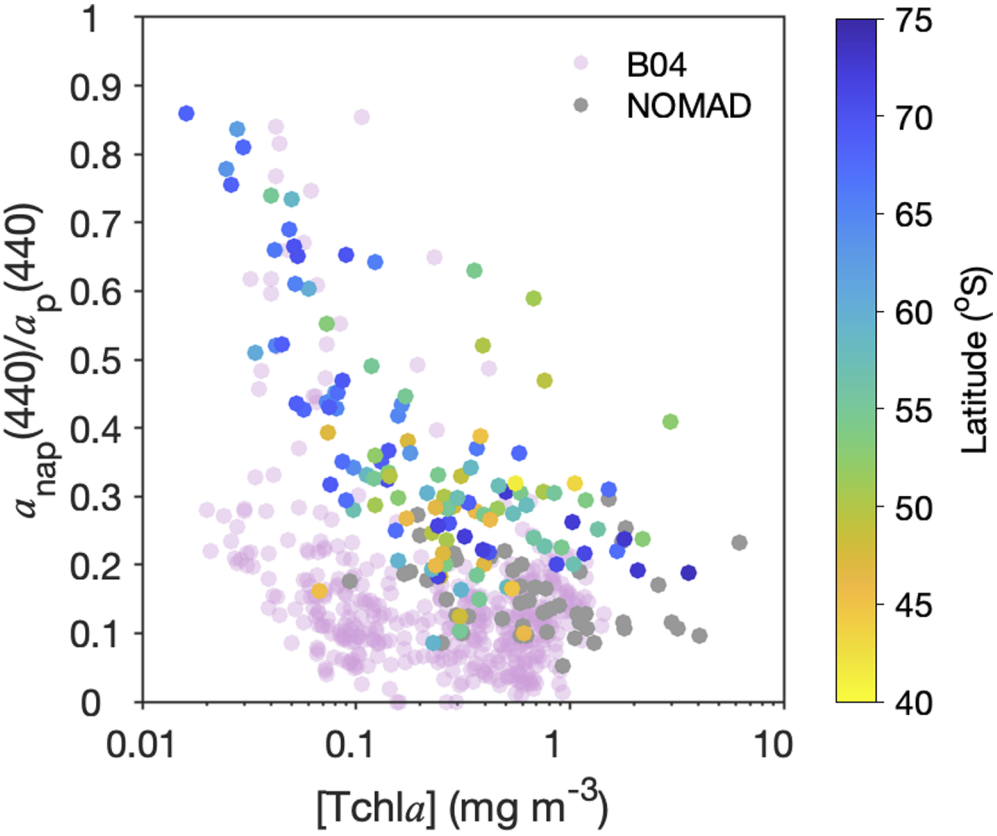

Fig. 16. Ratio of non-algal particulate absorption to total particulate absorption at 440 nm ($a_{nap}(440)/a_p(440)$) as a function of [Tchl$a$]. Datapoints are colourmapped by latitude. Data from B04 [53] are mauve points and from the NOMAD dataset are grey points.

4. Conclusion

Southern Ocean waters are optically unique [116], although much of the *in situ* bio-optical data collected in the SO so far has been spatially constrained. The ACE voyage gave us the opportunity to collect a unique dataset of phytoplankton particulate absorption, pigments and particle size across the entire longitudinal and latitudinal range of the SO. From this dataset, we confirm strikingly different relationships between chlorophyll-specific absorption and community composition and size when compared to other oceans (particularly in low wavelengths and at low chlorophyll *a* concentrations). In particular, we find high fractions of microplankton across all chlorophyll *a* concentrations and as a result, the phytoplankton absorption spectrum is flatter than other oceans at all chlorophyll *a*, and overall phytoplankton absorption and chlorophyll-specific absorption is lower than other oceans. Furthermore, we find considerable differences in the bio-optical relationships of high and low latitude phytoplankton in the SO. It is apparent from our work that interpreting ocean colour or other bio-optical signals in the SO with paradigms and parameterisations from lower latitude temperate oceans, such as the phytoplankton absorption spectral shape or composition of the phytoplankton community as a function of chlorophyll *a* can lead to incorrect conclusions.

Optics EXPRESS

In terms of optical budgets, this study focused on absorption terms and only measured particulate properties. It can be assumed that if chlorophyll-specific particulate absorption is lower in the Southern Ocean than other ocean basins, and is variable with latitude, and yet that satellite chlorophyll retrievals appear to be within acceptable uncertainties [117,118], then there may be some deviations in the chlorophyll-specific and particle-specific backscattering relationships, which has implications for the potential accurate satellite retrievals of particle size [119]. Additionally, patterns in a_{nap} show that high latitude locations deviate from a 'Case 1' waters optical scenario of a_{nap} varying strongly with chlorophyll a, and so it can be expected that there is also considerable spatial variability in absorption by coloured dissolved organic matter. We also show that pheopigments contribute substantially to the pigment biomass, especially at high latitudes, and may also contribute to particulate absorption at 676 nm.

It is clear from our work that relationships between phytoplankton pigments, particulate absorption and particle properties vary considerably within the SO, but can be parameterised with continued *in situ* observations across different biomes. We would also expect considerable intra- and inter-seasonal variability in these relationships as the phytoplankton composition and size responds to changes in mixing layer depth, light availability and access to dissolved iron and silicic acid, but capturing those changes *in situ* remains a logistical challenge.

Funding. Ferring Pharmaceuticals; Southern Ocean Carbon and Climate Observatory; Swiss Polar Institute; Council for Scientific and Industrial Research, South Africa (SNA2011112600001); Australian Research Council (DP160103387); Curtin University.

Acknowledgments. We would like to thank Annick Bricaud for providing datasets and all members of Project 1 from the Antarctic Circumnavigation Expedition, including William Moutier, David Berliner, Alexandra Olivier, and Hazel Little, as well as staff from the Swiss Polar Institute and the crew from the *RV* Akademik Trynoshnikov.

Disclosures. The authors declare no conflicts of interest.

Data availability. The datasets containing phytoplankton pigments can be found at Antoine et al. [51], particulate absorption at Antoine et al. [52], and photosynthetically active radiation at Thomalla et al. [48]. The dataset containing particle size distribution measurements will be made available at [120]. Other datasets from the Antarctic Circumpolar Expedition including latitude, longitude, thermosalinograph data, CTD and XBT (Haumann et al. [43] and Henry et al. [45]) data can be found at [120]. The power law relationships between phytoplankton absorption and chlorophyll a are available in Data File 1, Data File 2, and Data File 3.

Supplemental document. See Supplement 1 for supporting content.

References

1. T. L. Frölicher, J. L. Sarmiento, D. J. Paynter, J. P. Dunne, J. P. Krasting, and M. Winton, "Dominance of the southern ocean in anthropogenic carbon and heat uptake in cmip5 models," J. Climate **28**(2), 862–886 (2015).
2. T. Takahashi, S. C. Sutherland, R. Wanninkhof, C. Sweeney, R. A. Feely, D. W. Chipman, B. Hales, G. Friederich, F. Chavez, C. Sabine, A. Watson, D. C. Bakker, U. Scuster, N. Metzl, H. Yoshikawa-Inoue, M. Ishii, T. Midorikawa, Y. Nojiri, A. Kortzinger, T. Steinhoff, M. Hoppema, J. Olafsson, T. S. Arnarson, B. Tilbrook, T. Johannessen, A. Olse, R. Bellerby, C. Wong, B. Delille, N. Bates, and H. J. Baar, "Climatological mean and decadal change in surface ocean pco2, and net sea–air co2 flux over the global oceans," Deep Sea Res., Part II **56**(8-10), 554–577 (2009).
3. P. W. Boyd, S. C. Doney, R. Strzepek, J. Dusenberry, K. Lindsay, and I. Fung, "Climate-mediated changes to mixed-layer properties in the southern ocean: assessing the phytoplankton response," Biogeosciences **5**(3), 847–864 (2008).
4. A. J. Constable, J. Melbourne-Thomas, S. P. Corney, K. R. Arrigo, C. Barbraud, D. K. Barnes, N. L. Bindoff, P. W. Boyd, A. Brandt, D. P. Costa, A. T. Davidson, H. W. Ducklow, L. Emmerson, M. Fukuchi, J. Gutt, M. A. Hindell, E. E. Hofmann, G. W. Hosie, T. Iida, S. Jacob, N. M. Johnston, S. Kawaguchi, N. Kokubun, P. Koubbi, M.-A. Leo, A. Makhado, R. A. Masson, K. Meiners, M. P. Meredith, E. J. Murphy, S. Nicol, K. Reid, K. Richerson, M. J. Riddle, S. R. Rintoul, W. O. Smith Jr, C. Southwell, J. S. Stark, M. Sumner, K. M. Swadling, K. T. Takahashi, P. N. Trathan, D. C. Welsford, H. Weimerskirch, K. J. Westwood, B. C. Wienecke, D. Wolf-Gladrow, S. W. Wright, J. C. Xavier, and P. Ziegler, "Climate change and southern ocean ecosystems i: how changes in physical habitats directly affect marine biota," Glob Change Biol. **20**, 3004–3025 (2014).
5. K. Petrou, S. A. Kranz, S. Trimborn, C. S. Hassler, S. B. Ameijeiras, O. Sackett, P. J. Ralph, and A. T. Davidson, "Southern ocean phytoplankton physiology in a changing climate," J. Plant Physiol. **203**, 135–150 (2016).
6. M. Ardyna, H. Claustre, J.-B. Sallée, F. d'Ovidio, B. Gentili, G. Van Dijken, F. d'Ortenzio, and K. R. Arrigo, "Delineating environmental control of phytoplankton biomass and phenology in the southern ocean," Geophys. Res. Lett. **44**(10), 5016–5024 (2017).

Optics EXPRESS

7. S. Alvain, C. Moulin, Y. Dandonneau, and H. Loisel, "Seasonal distribution and succession of dominant phytoplankton groups in the global ocean: A satellite view," Global Biogeochem. Cycles **22**(3), GB3001 (2008).
8. K. R. Arrigo and G. L. Van Dijken, "Phytoplankton dynamics within 37 antarctic coastal polynya systems," J. Geophys. Res. **108**(C8), 3271 (2003).
9. C. Sullivan, K. Arrigo, C. McClain, J. Comiso, and J. Firestone, "Distributions of phytoplankton blooms in the southern ocean," Science **262**(5141), 1832–1837 (1993).
10. J. Uitz, H. Claustre, A. Morel, and S. B. Hooker, "Vertical distribution of phytoplankton communities in open ocean: An assessment based on surface chlorophyll," J. Geophys. Res. **111**(C8), C08005 (2006).
11. R. J. Brewin, S. Sathyendranath, T. Hirata, S. J. Lavender, R. M. Barciela, and N. J. Hardman-Mountford, "A three-component model of phytoplankton size class for the atlantic ocean," Ecological Modelling **221**(11), 1472–1483 (2010).
12. S. B. Groom, S. Sathyendranath, Y. Ban, S. Bernard, B. Brewin, V. Brotas, C. Brockmann, P. Chauhan, J.-K. Choi, A. Chuprin, S. Ciavatta, P. Cipollini, C. Donlon, B. Franz, X. He, T. Hirata, T. Jackson, M. Kampel, H. Krasemann, S. Lavender, S. Pardo-Martinez, F. Melin, T. Platt, R. Santoleri, J. Skakala, B. Schaeffer, M. Smith, F. Steinmetz, A. Valente, and M. Wang, "Satellite ocean colour: current status and future perspective," Front. Mar. Sci. **6**, 485 (2019).
13. S. Sathyendranath, R. J. Brewin, T. Jackson, F. Mélin, and T. Platt, "Ocean-colour products for climate-change studies: What are their ideal characteristics?" Remote Sensing of Environment **203**, 125–138 (2017).
14. D. A. Siegel, S. Maritorena, N. B. Nelson, and M. J. Behrenfeld, "Independence and interdependencies among global ocean color properties: Reassessing the bio-optical assumption," J. Geophys. Res. **110**(C7), C07011 (2005).
15. S. Sathyendranath, V. Stuart, B. D. Irwin, H. Maass, G. Savidge, L. Gilpin, and T. Platt, "Seasonal variations in bio-optical properties of phytoplankton in the arabian sea," Deep Sea Res., Part II **46**(3-4), 633–653 (1999).
16. C. Poulin, D. Antoine, and Y. Huot, "Diurnal variations of the optical properties of phytoplankton in a laboratory experiment and their implication for using inherent optical properties to measure biomass," Opt. Express **26**(2), 711–729 (2018).
17. R. Johnson, P. G. Strutton, S. W. Wright, A. McMinn, and K. M. Meiners, "Three improved satellite chlorophyll algorithms for the southern ocean," J. Geophys. Res. **118**(7), 3694–3703 (2013).
18. B. G. Mitchell and O. Holm-Hansen, "Bio-optical properties of antarctic peninsula waters: differentiation from temperate ocean models," Deep Sea Research Part A. Oceanographic Research Papers **38**(8-9), 1009–1028 (1991).
19. M. Kahru and B. G. Mitchell, "Blending of ocean colour algorithms applied to the southern ocean," Remote Sensing Letters **1**(2), 119–124 (2010).
20. L. A. Clementson, J. S. Parslow, A. R. Turnbull, D. C. McKenzie, and C. E. Rathbone, "Optical properties of waters in the australasian sector of the southern ocean," J. Geophys. Res. **106**(C12), 31611–31625 (2001).
21. A. Ferreira, V. M. Garcia, and C. A. Garcia, "Light absorption by phytoplankton, non-algal particles and dissolved organic matter at the patagonia shelf-break in spring and summer," Deep Sea Res., Part I **56**(12), 2162–2174 (2009).
22. A.-C. Alderkamp, M. M. Mills, G. L. van Dijken, P. Laan, C.-E. Thuróczy, L. J. Gerringa, H. J. de Baar, C. D. Payne, R. J. Visser, A. G. Buma, and K. R. Arrigo, "Iron from melting glaciers fuels phytoplankton blooms in the amundsen sea (southern ocean): Phytoplankton characteristics and productivity," Deep Sea Res., Part II **71-76**, 32–48 (2012).
23. R. A. Reynolds, D. Stramski, and B. G. Mitchell, "A chlorophyll-dependent semianalytical reflectance model derived from field measurements of absorption and backscattering coefficients within the southern ocean," J. Geophys. Res. **106**(C4), 7125–7138 (2001).
24. H. Dierssen, M. Vernet, and R. Smith, "Optimizing models for remotely estimating primary production in antarctic coastal waters," Antarctic Sci. **12**(1), 20–32 (2000).
25. A. U. Kerkar, S. Tripathy, P. Minu, N. Baranval, P. Sabu, S. Patra, R. Mishra, and A. Sarkar, "Variability in primary productivity and bio-optical properties in the indian sector of the southern ocean during an austral summer," Polar Biol. **43**(10), 1469–1492 (2020).
26. K. R. Arrigo, D. H. Robinson, D. L. Worthen, B. Schieber, and M. P. Lizotte, "Bio-optical properties of the southwestern ross sea," J. Geophys. Res. **103**(C10), 21683–21695 (1998).
27. A.-C. Alderkamp, G. L. van Dijken, K. E. Lowry, K. M. Lewis, H. L. Joy-Warren, W. van de Poll, P. Laan, L. Gerringa, T. O. Delmont, B. D. Jenkins, and K. R. Arrigo, "Effects of iron and light availability on phytoplankton photosynthetic properties in the ross sea," Mar. Ecol. Prog. Ser. **621**, 33–50 (2019).
28. K. R. Arrigo, M. M. Mills, L. R. Kropuenske, G. L. van Dijken, A.-C. Alderkamp, and D. H. Robinson, "Photophysiology in two major southern ocean phytoplankton taxa: photosynthesis and growth of phaeocystis antarctica and fragilariopsis cylindrus under different irradiance levels," Integrative and Comparative Biology **50**(6), 950–966 (2010).
29. B. Jena, "The effect of phytoplankton pigment composition and packaging on the retrieval of chlorophyll-a concentration from satellite observations in the southern ocean," International Journal of Remote Sensing **38**(13), 3763–3784 (2017).
30. N. Stambler, "Primary production, light absorption and quantum yields of phytoplankton from the bellingshausen and amundsen seas (antarctica)," Polar Biol. **26**(7), 438–451 (2003).
31. A. M. Ciotti, M. R. Lewis, and J. J. Cullen, "Assessment of the relationships between dominant cell size in natural phytoplankton communities and the spectral shape of the absorption coefficient," Limnol. Oceanogr. **47**(2), 404–417 (2002).

Optics EXPRESS

32. A. Bricaud and A. Morel, "Light attenuation and scattering by phytoplanktonic cells: a theoretical modeling," Appl. Opt. **25**(4), 571–580 (1986).
33. A. H. Orsi, T. Whitworth III, and W. D. Nowlin Jr, "On the meridional extent and fronts of the antarctic circumpolar current," Deep Sea Res., Part I **42**(5), 641–673 (1995).
34. C. C. Chapman, M.-A. Lea, A. Meyer, J.-B. Sallée, and M. Hindell, "Defining southern ocean fronts and their influence on biological and physical processes in a changing climate," Nat. Clim. Chang. **10**(3), 209–219 (2020).
35. S. Sokolov and S. R. Rintoul, "On the relationship between fronts of the antarctic circumpolar current and surface chlorophyll concentrations in the southern ocean," J. Geophys. Res. **112**(C7), C07030 (2007).
36. A. Ishikawa, S. W. Wright, R. van den Enden, A. T. Davidson, and H. J. Marchant, "Abundance, size structure and community composition of phytoplankton in the southern ocean in the austral summer 1999/2000," Polar Bioscience **15**, 11–26 (2002).
37. R. Eriksen, T. W. Trull, D. Davies, P. Jansen, A. T. Davidson, K. Westwood, and R. van den Enden, "Seasonal succession of phytoplankton community structure from autonomous sampling at the australian southern ocean time series (sots) observatory," Mar. Ecol. Prog. Ser. **589**, 13–31 (2018).
38. S. Honjo, "Particle export and the biological pump in the southern ocean," Antarctic Sci. **16**(4), 501–516 (2004).
39. C. Wolf, S. Frickenhaus, E. S. Kilias, I. Peeken, and K. Metfies, "Regional variability in eukaryotic protist communities in the amundsen sea," Antarctic Sci. **25**(6), 741–751 (2013).
40. P. W. Boyd, "The role of iron in the biogeochemistry of the southern ocean and equatorial pacific: a comparison of in situ iron enrichments," Deep Sea Res., Part II **49**(9-10), 1803–1821 (2002).
41. P. W. Boyd, A. J. Watson, C. S. Law, E. R. Abraham, T. Trull, R. Murdoch, D. C. Bakker, A. R. Bowie, K. Buesseler, H. Chang, M. Charette, P. Croot, K. Downing, R. Frew, M. Gall, M. Hadfield, J. Hall, M. Harvey, G. Jameson, J. LaRoche, M. Liddicoat, R. Ling, M. T. Maldonado, R. M. Mckay, S. Nodder, S. Pickmere, R. Prodmore, S. Rintoul, K. Safi, P. Sutton, R. Strzepek, K. Tanneberger, S. Turner, A. Waite, and J. Zeldis, "A mesoscale phytoplankton bloom in the polar southern ocean stimulated by iron fertilization," Nature **407**(6805), 695–702 (2000).
42. D. W. H. Walton and J. Thomas, "Cruise Report - Antarctic Circumnavigation Expedition (ACE) 20th December 2016 - 19th March 2017," https://doi.org/10.5281/zenodo.1443511 (2018).
43. F. A. Haumann, C. Robinson, J. Thomas, J. Hutchings, C. Pina Estany, A. Tarasenko, F. Gerber, and K. Leonard, "Physical and biogeochemical oceanography data from underway measurements with an AquaLine Ferrybox during the Antarctic Circumnavigation Expedition (ACE).," Zenodo, 2020, https://doi.org/10.5281/zenodo.3660852 .
44. C. de Boyer Montégut, G. Madec, A. S. Fischer, A. Lazar, and D. Iudicone, "Mixed layer depth over the global ocean: An examination of profile data and a profile-based climatology," J. Geophys. Res. **109**(C12), C12003 (2004).
45. T. Henry, C. Robinson, F. A. Haumann, J. Thomas, J. Hutchings, N. Schuback, M. Tsukernik, and K. Leonard, "Physical and biogeochemical oceanography data from Conductivity, Temperature, Depth (CTD) rosette deployments during the Antarctic Circumnavigation Expedition (ACE)," Zenodo, 2020, https://doi.org/10.5281/zenodo.3813646.
46. A. Morel, Y. Huot, B. Gentili, P. J. Werdell, S. B. Hooker, and B. A. Franz, "Examining the consistency of products derived from various ocean color sensors in open ocean (case 1) waters in the perspective of a multi-sensor approach," Remote Sensing of Environment **111**(1), 69–88 (2007).
47. A. Morel, "Optical modeling of the upper ocean in relation to its biogenous matter content (case i waters)," J. Geophys. Res. **93**(C9), 10749–10768 (1988).
48. S. Thomalla, D. Antoine, D. Berliner, H. Little, W. Moutier, A. Olivier-Morgan, C. Robinson, T. Ryan-Keogh, and N. Schuback, "Sky irradiance over photosynthetically active radiation wavelengths (400-700 nm) recorded shipboard during the Antarctic Circumnavigation Expedition (ACE) during the Austral Summer of 2016/2017.," https://doi.org/10.5281/zenodo.3859836 (2020).
49. J. T. Kirk, *Light and photosynthesis in aquatic ecosystems* (Cambridge university, 1994).
50. J. Ras, H. Claustre, and J. Uitz, "Spatial variability of phytoplankton pigment distributions in the subtropical south pacific ocean: comparison between in situ and predicted data," Biogeosciences **5**(2), 353–369 (2008).
51. D. Antoine, S. Thomalla, D. Berliner, H. Little, W. Moutier, A. Olivier-Morgan, C. Robinson, T. Ryan-Keogh, and N. Schuback, "Phytoplankton pigment concentrations of seawater sampled during the Antarctic Circumnavigation Expedition (ACE) during the Austral Summer of 2016/2017.," Zenodo, 2020, https://doi.org/10.5281/zenodo.3816726.
52. D. Antoine, S. Thomalla, D. Berliner, H. Little, W. Moutier, A. Olivier-Morgan, C. Robinson, T. Ryan-Keogh, and N. Schuback, "Particulate light absorption coefficients (350 – 750 nm) measured using the filter pad method during the Antarctic Circumnavigation Expedition (ACE) during the austral summer of 2016/2017," Zenodo, 2020, https://zenodo.org/record/3993096.
53. A. Bricaud, H. Claustre, J. Ras, and K. Oubelkheir, "Natural variability of phytoplanktonic absorption in oceanic waters: Influence of the size structure of algal populations," J. Geophys. Res. **109**(C11), C11010 (2004).
54. A. Bricaud, M. Babin, H. Claustre, J. Ras, and F. Tièche, "Light absorption properties and absorption budget of southeast pacific waters," J. Geophys. Res. **115**(C8), C08009 (2010).
55. T. F. Coleman and Y. Li, "On the convergence of interior-reflective newton methods for nonlinear minimization subject to bounds," Mathematical programming **67**(1-3), 189–224 (1994).
56. T. F. Coleman and Y. Li, "An interior trust region approach for nonlinear minimization subject to bounds," SIAM J. Optim. **6**(2), 418–445 (1996).
57. H. Claustre, "The trophic status of various oceanic provinces as revealed by phytoplankton pigment signatures," Limnol. Oceanogr. **39**(5), 1206–1210 (1994).

Optics EXPRESS

58. F. Vidussi, H. Claustre, B. B. Manca, A. Luchetta, and J.-C. Marty, "Phytoplankton pigment distribution in relation to upper thermocline circulation in the eastern mediterranean sea during winter," J. Geophys. Res. **106**(C9), 19939–19956 (2001).
59. L. A. Clementson and B. Wojtasiewicz, "Dataset on the in vivo absorption characteristics and pigment composition of various phytoplankton species," Data in Brief **25**, 104020 (2019).
60. M. E. Baird, M. Mongin, F. Rizwi, L. K. Bay, N. E. Cantin, M. Soja-Woźniak, and J. Skerratt, "A mechanistic model of coral bleaching due to temperature-mediated light-driven reactive oxygen build-up in zooxanthellae," Ecological Modelling **386**, 20–37 (2018).
61. L. Garcia-Rubio, "Refractive index effects on the absorption spectra of macromolecules," Macromolecules **25**(10), 2608–2613 (1992).
62. R. R. Bidigare, M. E. Ondrusek, J. H. Morrow, and D. A. Kiefer, "In-vivo absorption properties of algal pigments," in *Ocean Optics X*, vol. 1302 (International Society for Optics and Photonics, 1990), pp. 290–302.
63. P. J. Werdell and S. W. Bailey, "An improved in-situ bio-optical data set for ocean color algorithm development and satellite data product validation," Remote Sensing of Environment **98**(1), 122–140 (2005).
64. A. Bricaud, A. Morel, M. Babin, K. Allali, and H. Claustre, "Variations of light absorption by suspended particles with chlorophyll a concentration in oceanic (case 1) waters: Analysis and implications for bio-optical models," J. Geophys. Res. **103**(C13), 31033–31044 (1998).
65. G. A. Knox, *Biology of the Southern Ocean* (Taylor & Francis Group, LLC, Boca Raton, Florida, 2006), chap. 1, pp. 1–16, 2nd ed.
66. D. F. Porter, S. R. Springer, L. Padman, H. A. Fricker, K. J. Tinto, S. C. Riser, R. E. Bell, and R.-I. Team, "Evolution of the seasonal surface mixed layer of the ross sea, antarctica, observed with autonomous profiling floats," J. Geophys. Res. **124**(7), 4934–4953 (2019).
67. M. Mongin, E. Molina, and T. W. Trull, "Seasonality and scale of the kerguelen plateau phytoplankton bloom: A remote sensing and modeling analysis of the influence of natural iron fertilization in the southern ocean," Deep Sea Res., Part II **55**(5-7), 880–892 (2008).
68. Y.-H. Park, F. Roquet, I. Durand, and J.-L. Fuda, "Large-scale circulation over and around the northern kerguelen plateau," Deep Sea Res., Part II **55**(5-7), 566–581 (2008).
69. M. Klunder, P. Laan, R. Middag, H. De Baar, and J. Van Ooijen, "Dissolved iron in the southern ocean (atlantic sector)," Deep Sea Res., Part II **58**(25-26), 2678–2694 (2011).
70. J. H. Martin, M. Gordon, and S. E. Fitzwater, "The case for iron," Limnol. Oceanogr. **36**(8), 1793–1802 (1991).
71. R. E. Korb and M. Whitehouse, "Contrasting primary production regimes around south georgia, southern ocean: large blooms versus high nutrient, low chlorophyll waters," Deep Sea Res., Part I **51**(5), 721–738 (2004).
72. P. W. Boyd, T. Jickells, C. Law, S. Blain, E. Boyle, K. Buesseler, K. Coale, J. Cullen, H. J. De Baar, M. Follows, M. Harvey, C. Lancelot, M. Levasseur, N. P. J. Owens, R. Pollard, R. B. Rivkin, J. Sarmiento, V. Schoemann, V. Smetacek, S. Takeda, A. Tsuda, S. Turner, and A. J. Watson, "Mesoscale iron enrichment experiments 1993-2005: synthesis and future directions," Science **315**(5812), 612–617 (2007).
73. A. Morel, B. Gentili, H. Claustre, M. Babin, A. Bricaud, J. Ras, and F. Tieche, "Optical properties of the – clearest – natural waters," Limnol. Oceanogr. **52**(1), 217–229 (2007).
74. S. Blain, B. Quéguiner, L. Armand, S. Belviso, B. Bombled, L. Bopp, A. Bowie, C. Brunet, C. Brussaard, F. Carlotti, U. Christaki, A. Corbiere, I. Durand, F. Ebersback, J.-L. Fuda, N. Garcia, L. Gerringa, B. Griffiths, C. Guigue, C. Guillerm, S. Jacquet, C. Jeandel, P. Laan, D. Lefevre, C. L. Monaco, A. Malits, J. Mosseri, I. Obernosterer, Y.-H. Park, M. Picheral, P. Pondaven, T. Remenyi, V. Sandroni, G. Sarthou, N. Savoye, L. Scouarnec, M. Souhaut, D. Thuiller, K. Timmermans, T. Trull, J. Uitz, P. van Beek, M. Veldhuis, D. Vincent, E. Viollier, L. Vong, and T. Wagener, "Effect of natural iron fertilization on carbon sequestration in the southern ocean," Nature **446**(7139), 1070–1074 (2007).
75. S. Blain, G. Sarthou, and P. Laan, "Distribution of dissolved iron during the natural iron-fertilization experiment keops (kerguelen plateau, southern ocean)," Deep Sea Res., Part II **55**(5-7), 594–605 (2008).
76. R. Perissinotto, R. Laubscher, and C. McQuaid, "Marine productivity enhancement around bouvet and the south sandwich islands (southern ocean)," Mar. Ecol. Prog. Ser. **88**, 41–53 (1992).
77. O. Holm-Hansen, M. Kahru, C. Hewes, S. Kawaguchi, T. Kameda, V. Sushin, I. Krasovski, J. Priddle, R. Korb, R. Hewitt, and B. Mitchell, "Temporal and spatial distribution of chlorophyll-a in surface waters of the scotia sea as determined by both shipboard measurements and satellite data," Deep Sea Res., Part II **51**(12-13), 1323–1331 (2004).
78. J. Park, I.-S. Oh, H.-C. Kim, and S. Yoo, "Variability of seawifs chlorophyll-a in the southwest atlantic sector of the southern ocean: Strong topographic effects and weak seasonality," Deep Sea Res., Part I **57**(4), 604–620 (2010).
79. A. L. Rivas, A. I. Dogliotti, and D. A. Gagliardini, "Seasonal variability in satellite-measured surface chlorophyll in the patagonian shelf," Continental Shelf Research **26**(6), 703–720 (2006).
80. S. Blain, P. Tréguer, S. Belviso, E. Bucciarelli, M. Denis, S. Desabre, M. Fiala, V. M. Jézéquel, J. Le Fèvre, P. Mayzaud, J.-C. Marty, and S. Razouls, "A biogeochemical study of the island mass effect in the context of the iron hypothesis: Kerguelen islands, southern ocean," Deep Sea Res., Part I **48**(1), 163–187 (2001).
81. J. R. Hawkings, J. L. Wadham, M. Tranter, R. Raiswell, L. G. Benning, P. J. Statham, A. Tedstone, P. Nienow, K. Lee, and J. Telling, "Ice sheets as a significant source of highly reactive nanoparticulate iron to the oceans," Nat. Commun. **5**(1), 3929 (2014).
82. A. Bricaud, M. Babin, A. Morel, and H. Claustre, "Variability in the chlorophyll-specific absorption coefficients of natural phytoplankton: Analysis and parameterization," J. Geophys. Res. **100**(C7), 13321–13332 (1995).

Optics EXPRESS

83. C. R. B. Mendes, R. Kerr, V. M. Tavano, F. A. Cavalheiro, C. A. E. Garcia, D. R. G. Dessai, and N. Anilkumar, "Cross-front phytoplankton pigments and chemotaxonomic groups in the indian sector of the southern ocean," Deep Sea Res., Part II **118**, 221–232 (2015).
84. S. W. Wright, R. L. van den Enden, I. Pearce, A. T. Davidson, F. J. Scott, and K. J. Westwood, "Phytoplankton community structure and stocks in the southern ocean (30–80 e) determined by chemtax analysis of hplc pigment signatures," Deep Sea Res., Part II **57**(9-10), 758–778 (2010).
85. S. Jeffrey, "Profiles of photosynthetic pigments in the ocean using thin-layer chromatography," Marine Biol. **26**(2), 101–110 (1974).
86. N. M. Freeman, N. S. Lovenduski, D. R. Munro, K. M. Krumhardt, K. Lindsay, M. C. Long, and M. Maclennan, "The variable and changing southern ocean silicate front: insights from the cesm large ensemble," Global Biogeochem. Cycles **32**(5), 752–768 (2018).
87. N. Cassar, S. W. Wright, P. G. Thomson, T. W. Trull, K. J. Westwood, M. de Salas, A. Davidson, I. Pearce, D. M. Davies, and R. J. Matear, "The relation of mixed-layer net community production to phytoplankton community composition in the southern ocean," Global Biogeochem. Cycles **29**(4), 446–462 (2015).
88. H. Liu, R. R. Bidigare, E. Laws, M. R. Landry, and L. Campbell, "Cell cycle and physiological characteristics of synechococcus (wh7803) in chemostat culture," Mar. Ecol. Prog. Ser. **189**, 17–25 (1999).
89. P. W. Boyd, "Environmental factors controlling phytoplankton processes in the southern ocean1," J. Phycol. **38**(5), 844–861 (2002).
90. A. Goffart, G. Catalano, and J.-H. Hecq, "Factors controlling the distribution of diatoms and phaeocystis in the ross sea," J. Marine Systems **27**(1-3), 161–175 (2000).
91. K. R. Arrigo, D. L. Worthen, and D. H. Robinson, "A coupled ocean-ecosystem model of the ross sea: 2. iron regulation of phytoplankton taxonomic variability and primary production," J. Geophys. Res. **108**(C7), 3231 (2003).
92. M. A. Moline and B. B. Prezelin, "Long-term monitoring and analyses of physical factors regulating variability in coastal antarctic phytoplankton biomass, in situ productivity and taxonomic composition over subseasonal, seasonal and interannual time scales," Mar. Ecol. Prog. Ser. **145**, 143–160 (1996).
93. H. Claustre, M. A. Moline, and B. B. Prézelin, "Sources of variability in the column photosynthetic cross section for antarctic coastal waters," J. Geophys. Res. **102**(C11s), 25047–25060 (1997).
94. D. J. Janssen, M. Sieber, M. J. Ellwood, T. M. Conway, P. M. Barrett, X. Chen, G. F. de Souza, C. S. Hassler, and S. L. Jaccard, "Trace metal and nutrient dynamics across broad biogeochemical gradients in the indian and pacific sectors of the southern ocean," Marine chemistry **221**, 103773 (2020).
95. H. Venables and C. M. Moore, "Phytoplankton and light limitation in the southern ocean: Learning from high-nutrient, high-chlorophyll areas," J. Geophys. Res. **115**(C2), C02015 (2010).
96. R. F. Strzepek, M. T. Maldonado, K. A. Hunter, R. D. Frew, and P. W. Boyd, "Adaptive strategies by southern ocean phytoplankton to lessen iron limitation: Uptake of organically complexed iron and reduced cellular iron requirements," Limnol. Oceanogr. **56**(6), 1983–2002 (2011).
97. C. D. Hewes, "Cell size of antarctic phytoplankton as a biogeochemical condition," Antarctic Sci. **21**(5), 457–470 (2009).
98. M. Varela, E. Fernandez, and P. Serret, "Size-fractionated phytoplankton biomass and primary production in the gerlache and south bransfield straits (antarctic peninsula) in austral summer 1995–1996," Deep Sea Res., Part II **49**(4-5), 749–768 (2002).
99. S. W. Chisholm, "Phytoplankton size," in *Primary productivity and biogeochemical cycles in the sea*, (Springer, 1992), pp. 213–237.
100. K. Petrou, C. S. Hassler, M. A. Doblin, K. Shelly, V. Schoemann, R. van den Enden, S. Wright, and P. J. Ralph, "Iron-limitation and high light stress on phytoplankton populations from the australian sub-antarctic zone (saz)," Deep Sea Res., Part II **58**(21-22), 2200–2211 (2011).
101. W. Cheah, A. McMinn, F. B. Griffiths, K. J. Westwood, S. W. Wright, and L. A. Clementson, "Response of phytoplankton photophysiology to varying environmental conditions in the sub-antarctic and polar frontal zone," PLoS One **8**(8), e72165 (2013).
102. S. M. Andrew, H. T. Morell, R. F. Strzepek, P. W. Boyd, and M. J. Ellwood, "Iron availability influences the tolerance of southern ocean phytoplankton to warming and elevated irradiance," Front. Mar. Sci. **6**, 681 (2019).
103. A. Morel and A. Bricaud, "Theoretical results concerning light absorption in a discrete medium, and application to specific absorption of phytoplankton," Deep Sea Research Part A. Oceanographic Research Papers **28**(11), 1375–1393 (1981).
104. R. J. Brewin, G. Dall-Olmo, S. Sathyendranath, and N. J. Hardman-Mountford, "Particle backscattering as a function of chlorophyll and phytoplankton size structure in the open-ocean," Opt. Express **20**(16), 17632–17652 (2012).
105. X. Zhang, L. Hu, Y. Xiong, Y. Huot, and D. Gray, "Experimental estimates of optical backscattering associated with submicron particles in clear oceanic waters," Geophys. Res. Lett. **47**(4), e2020GL087100 (2020).
106. T. Y. Churilova, G. Berseneva, and L. Georgieva, "Variability of the biooptical characteristics of phytoplankton in the black sea," Oceanology **44**, 192–204 (2004).
107. S. Wang, J. Ishizaka, H. Yamaguchi, S. Tripathy, M. Hayashi, Y. Xu, Y. Mino, T. Matsuno, Y. Watanabe, and S. Yoo, "Influence of the changjiang river on the light absorption properties of phytoplankton from the east china sea," Biogeosciences **11**(7), 1759–1773 (2014).

Optics EXPRESS

108. T. A. Moisan and B. G. Mitchell, "Photophysiological acclimation of phaeocystis antarctica karsten under light limitation," Limnol. Oceanogr. **44**(2), 247–258 (1999).
109. N. Nelson and B. Prézelin, "Chromatic light effects and physiological modeling of absorption properties heterocapsa pygmaea (= glenodinium sp.)," Mar. Ecol. Prog. Ser. **63**, 37–46 (1990).
110. G. Johnsen, N. B. Nelson, R. V. Jovine, and B. B. Prezelin, "Chromoprotein-and pigment-dependent modeling of spectral light absorption in two dinoflagellates, prorocentrum minimum and heterocapsa pygmaea," Mar. Ecol. Prog. Ser. **114**, 245–258 (1994).
111. G. L. Pérez, M. Galí, S.-J. Royer, M. Gerea, E. Ortega-Retuerta, J. M. Gasol, C. Marrasé, and R. Simó, "Variability of phytoplankton light absorption in stratified waters of the nw mediterranean sea: the interplay between pigment composition and the packaging effect," Deep Sea Res., Part I **169**, 103460 (2021).
112. A. Bricaud and D. Stramski, "Spectral absorption coefficients of living phytoplankton and nonalgal biogenous matter: A comparison between the peru upwelling areaand the sargasso sea," Limnol. Oceanogr. **35**(3), 562–582 (1990).
113. M. Kishino, M. Takahashi, N. Okami, and S. Ichimura, "Estimation of the spectral absorption coefficients of phytoplankton in the sea," Bulletin of Marine Science **37**(2), 634–642 (1985).
114. R. Röttgers and S. Gehnke, "Measurement of light absorption by aquatic particles: improvement of the quantitative filter technique by use of an integrating sphere approach," Appl. Opt. **51**(9), 1336–1351 (2012).
115. D. Stramski, R. A. Reynolds, S. Kaczmarek, J. Uitz, and G. Zheng, "Correction of pathlength amplification in the filter-pad technique for measurements of particulate absorption coefficient in the visible spectral region," Appl. Opt. **54**(22), 6763–6782 (2015).
116. M. Szeto, P. Werdell, T. Moore, and J. Campbell, "Are the world's oceans optically different?" J. Geophys. Res. **116**(C7), 2011JC007230 (2011).
117. W. Moutier, S. J. Thomalla, S. Bernard, G. Wind, T. J. Ryan-Keogh, and M. E. Smith, "Evaluation of chlorophyll-a and poc modis aqua products in the southern ocean," Remote Sensing **11**(15), 1793 (2019).
118. N. Haëntjens, E. Boss, and L. D. Talley, "Revisiting ocean color algorithms for chlorophyll a and particulate organic carbon in the southern ocean using biogeochemical floats," J. Geophys. Res. **122**(8), 6583–6593 (2017).
119. T. Kostadinov, D. Siegel, and S. Maritorena, "Retrieval of the particle size distribution from satellite ocean color observations," J. Geophys. Res. **114**(C9), C09015 (2009).
120. Zenodo, "Swiss Polar Institute: Antarctic Circumnavigation Expedition (ACE)," Zenodo, 2020, https://zenodo.org/communities/spi-ace.